AGU PUBLICATIONS

JGR

Journal of Geophysical Research: Atmospheres

RESEARCH ARTICLE

10.1002/2015JD024020

**Key Points:**
- PM1 concentrations are consistently high in recent years of Beijing (60 to 85 μg m$^{-3}$)
- Emission sources and formation pathways of aerosol in Beijing are seasonally different
- Cooking as nonfossil OA source (13–24%) is important in Beijing

**Supporting Information:**
- Texts S1–S4, Tables S1–S9, and Figures S1–S34

**Correspondence to:**
M. Hu,
minhu@pku.edu.cn

**Citation:**
Hu, W. W., et al. (2016), Chemical composition, sources, and aging process of submicron aerosols in Beijing: Contrast between summer and winter, *J. Geophys. Res. Atmos.*, *121*, 1955–1977, doi:10.1002/2015JD024020.

Received 30 JUL 2015
Accepted 20 JAN 2016
Accepted article online 22 JAN 2016
Published online 26 FEB 2016



# Chemical composition, sources, and aging process of submicron aerosols in Beijing: Contrast between summer and winter

**Weiwei Hu[1,2], Min Hu[1], Wei Hu[1], Jose L. Jimenez[3,4], Bin Yuan[1,2,5], Wentai Chen[1], Ming Wang[1], Yusheng Wu[1], Chen Chen[1], Zhibin Wang[1,6], Jianfei Peng[1], Limin Zeng[1], and Min Shao[1]**

[1]State Key Joint Laboratory of Environmental Simulation and Pollution Control, College of Environmental Sciences and Engineering, Peking University, Beijing, China, [2]Now at Cooperative Institute for Research in Environmental Sciences, University of Colorado Boulder, Boulder, Colorado, USA, [3]Cooperative Institute for Research in the Environmental Sciences, Boulder, Colorado, USA, [4]Department of Chemistry and Biochemistry, University of Colorado Boulder, Boulder, Colorado, USA, [5]Now at Chemical Sciences Division, Earth System Research Laboratory, Boulder, Colorado, USA, [6]Now at Multiphase Chemistry Department, Max Planck Institute for Chemistry, Mainz, Germany

**Abstract** To investigate the seasonal characteristics of submicron aerosol ($PM_1$) in Beijing urban areas, a high-resolution time-of-flight aerosol-mass-spectrometer (HR-ToF-AMS) was utilized at an urban site in summer (August to September 2011) and winter (November to December 2010), coupled with multiple state of the art online instruments. The average mass concentrations of $PM_1$ (60–84 μg m$^{-3}$) and its chemical compositions in different campaigns of Beijing were relatively consistent in recent years. In summer, the daily variations of $PM_1$ mass concentrations were stable and repeatable. Eighty-two percent of the $PM_1$ mass concentration on average was composed of secondary species, where 62% is secondary inorganic aerosol and 20% secondary organic aerosol (SOA). In winter, $PM_1$ mass concentrations changed dramatically because of the different meteorological conditions. The high average fraction (58%) of primary species in $PM_1$ including primary organic aerosol (POA), black carbon, and chloride indicates primary emissions usually played a more important role in the winter. However, aqueous chemistry resulting in efficient secondary formation during occasional periods with high relative humidity may also contribute substantially to haze in winter. Results of past OA source apportionment studies in Beijing show 45–67% of OA in summer and 22–50% of OA in winter can be composed of SOA. Based on the source apportionment results, we found 45% POA in winter and 61% POA in summer are from nonfossil sources, contributed by cooking OA in both seasons and biomass burning OA (BBOA) in winter. Cooking OA, accounting for 13–24% of OA, is an important nonfossil carbon source in all years of Beijing and should not be neglected. The fossil sources of POA include hydrocarbon-like OA from vehicle emissions in both seasons and coal combustion OA (CCOA) in winter. The CCOA and BBOA were the two main contributors (57% of OA) for the highest OA concentrations (>100 μg m$^{-3}$) in winter. The POA/ΔCO ratios in winter and summer are 11 and 16 μg m$^{-3}$ ppm$^{-1}$, respectively, similar to ratios from western cities. Higher OOA/$O_x$ (= $NO_2 + O_3$) ratio (0.49 μg m$^{-3}$ ppb$^{-1}$) in winter study than these ratios from western cities (0.03–0.16 μg m$^{-3}$ ppb$^{-1}$) was observed, which may be due to the aqueous reaction or extra SOA formation contributed by semivolatile organic compounds from various primary sources (e.g., BBOA or CCOA) in Beijing. The evolution of oxygen to carbon ratio (O/C) with photochemical age allows to estimate an equivalent rate constant for chemical aging of OA in summer as $k_{OH} \sim 4.1 \times 10^{-12}$ cm$^3$ molecule$^{-1}$ s$^{-1}$, which is of the same order as obtained in other anthropogenic influenced areas and may be useful for OA modeling.

## 1. Introduction

Fine particles ($PM_{2.5}$ or $PM_1$, i.e., the particulate matter with aerodynamic diameter less than 2.5 μm or 1 μm) have significantly impacted on visibility reduction, climate change, and health concerns. As one of the largest megacities in the world, Beijing has quite severe air pollution because of rapid urbanization, motorization, and energy consumption in the last decade [*Huang et al.*, 2006; *Streets et al.*, 2007; *Huang et al.*, 2014]. In recent decades, high $PM_{2.5}$ concentrations (37–367 μg m$^{-3}$) were observed frequently across the whole year of Beijing, exceeding the Ambient Air Quality Standards of China and U.S. (75 μg m$^{-3}$ and 35 μg m$^{-3}$ for 24 h average, respectively) [*He et al.*, 2001; *Chan et al.*, 2005; *Huang et al.*, 2010; *Sun et al.*, 2010, 2013; *Wang et al.*, 2015]. The heavy air pollution condition in Beijing and its effect on human health have drawn more and more public attentions [*Guo et al.*, 2013; *Lovett*, 2013; *Sheehan et al.*, 2014].

A better understanding of the sources and chemical composition of fine particles is crucial to air pollution control and policy making. Multiple measurements have been carried out to investigate aerosols around Beijing. Organic aerosol (OA) can account for 20–60% of the total fine aerosol mass concentrations [*Sun et al*., 2004; *Duan et al*., 2005; *Zheng et al*., 2005; *Huang et al*., 2006; *Takegawa et al*., 2009]. Biomass burning, coal combustion, vehicle emission, cooking, and the secondary formation from anthropogenic precursors have been identified as important sources of fine particle in the Beijing area [*He et al*., 2001; *Zheng et al*., 2005; *Song et al*., 2006; *Sun et al*., 2013; *Guo et al*., 2014; *Huang et al*., 2014; *Zhang et al*., 2014]. Biogenic precursors mainly from isoprene and monoterpene could contribute SOA formation in Beijing as aerosol products (e.g., 2-methyltetrols and 2-methylglyceric acid) from isoprene oxidation and those (e.g., pinonic acid) from monoterpene oxidation; however, in relative low fractions [*Liang et al*., 2012; *Yuan et al*., 2012], for example, the average mass concentration of OA in $PM_1$ is on the order of several tens of $\mu g\,m^{-3}$, whereas the detected methyltetrols is usually $< 1\,\mu g\,m^{-3}$. Those sources show distinctive seasonal variations due to different meteorology and anthropogenic activities [*Zheng et al*., 2005; *Wang et al*., 2009; *Li et al*., 2015].

Aerosol mass spectrometers (AMS) are widely used for their fast time resolution (seconds to minutes) and ability to characterize the main species in submicron aerosols [*Canagaratna et al*., 2007; *Jimenez et al*., 2009; *Huang et al*., 2010]. Multiple OA sources can be distinguished and recognized by combining source apportionment method (e.g., positive matrix factorization (PMF)) with the high-resolution OA mass spectral matrix [*Ulbrich et al*., 2009]. Several results based on AMS measurements in the Beijing area have been reported [*Takegawa et al*., 2009; *Huang et al*., 2010; *Sun et al*., 2010, 2012, 2013; *Zhang et al*., 2014]. However, most of the results are based on unit mass resolution ($m/\Delta m = 1$, with $m$ being the nominal $m/z$ and $\Delta m$ being full width at half maximum) mass spectra from quadrupole mass spectrometers, or only focus on single season measurement. AMS with time-of-flight detectors (ToF-AMS) can measure ions at much higher resolutions ($m/\Delta m = 3000$–5000), which allows the elemental composition (e.g., C, H, O, and N) of many ions to be determined [*DeCarlo et al*., 2006]. Few results on evolution/aging processes of OA have been reported for the Beijing area, which would be useful for comparison with other urban areas and for secondary OA modeling work in Beijing.

In this study, two intensive campaigns were conducted to investigate the seasonal characteristics of fine particles in the winter and summer of Beijing. The time series, chemical composition, and size distributions of different species in fine particles are investigated based on HR-ToF-AMS measurement in both seasons. Then we obtained a detailed source apportionment result of OA by applying factor analysis to the time series of high-resolution organic spectral matrix. Results are compared to previous studies published in recent years for Beijing. Finally, we studied the ambient OA aging processes through combining oxidation level of OA (oxygen to carbon ratio = O/C; organic aerosol to organic carbon ratio = OA/OC) with photochemical age estimated from volatile organic compounds (VOCs) measurements.

## 2. Experiments

### 2.1. Sampling Site and Measurements

Winter (22 November to 22 December 2010) and summer (3 August to 15 September 2011) studies were conducted at PKU Urban Atmosphere Environment MonitoRing Station (PKUERS) (39.99°N, 116.31°E). This observation site is located on the roof of a six-story building (15 m above the ground) in the campus of Peking University located in the northwest of the fourth ring road. Detailed descriptions of this site can be obtained in several published papers [*Wu et al*., 2007; *Huang et al*., 2010].

### 2.2. The Operation and Data Analysis of HR-ToF-AMS

An HR-ToF-AMS (Aerodyne Research Inc., USA), hereafter termed as "AMS," can measure mass concentrations and size distributions of submicron nonrefractory species ($PM_1^{nr}$), i.e., OA, sulfate, nitrate, ammonium, and chloride. This instrument has been described previously in the literature [*DeCarlo et al*., 2006; *Canagaratna et al*., 2007], so only a brief summary of the aspects specific to our studies is given here.

Ambient air was sampled through a $PM_{2.5}$ cut cyclone (1.5 m above the roof) and a 3 m long 3/8 inch copper tube at $10\,L\,min^{-1}$; then a subset of the flow was subsampled toward the AMS instrument at $0.1\,L\,min^{-1}$. A nafion dryer before the AMS kept the relative humidity (RH) of the sampled air below 30%. The time resolution of AMS data in both studies is 4 min, with 2 min in V mode for $PM_1^{nr}$ mass and size distributions and 2 min in W mode for highest resolution mass spectra. Ionization efficiency (IE) calibrations were done every 5–7 days by

sampling monodispersed 400 nm dried pure ammonium nitrate particles into AMS. Those ammonium nitrate particles were generated by aerosol atomizer (3076, TSI Inc., USA) and selected with a differential mobility analyzer (DMA, model 3081, TSI Inc., USA). IE values obtained from Brute-Force Single-Particle method were used here. The ratio of IE to airbeam signal (= IE/AB, AB is referred to $N_2^+$ ion detected in AMS) of each calibration was used for converting the instrument signals to ambient mass concentrations. The IE/AB calibration values within the interval of two calibrations were obtained by linear interpreting IE/AB values before and after. Unless there was an instrument failure (e.g., turbo pump down), last good calibrated IE/AB value was used till the instrument failure time. The variability of IE/AB in both campaigns is within 15% uncertainty of average value (Figure S1 in the supporting information). Size calibrations were performed before and after each study by sampling into the AMS pure nitrate ammonium particles (50–550 nm) with a DMA and monodisperse polystyrene latex spheres (density = 1.05 g $cm^{-3}$) (Duke Scientific, U.S.) with nominal standard diameters of 100–700 nm.

Particle collection efficiency (CE) is needed to account for particle bounce losses on the AMS vaporizer ($E_b$) as a function of particle size [*Canagaratna et al*., 2007]. In this study, the chemical composition-based estimation of CE was estimated and used, following the method addressed in *Middlebrook et al*. [2012]. The average CE in both campaigns is around 0.5. The calculated CE only reach 0.6 during two short periods (several hours on 11 September) in summer study due to slightly high ammonium nitrate fraction in aerosols, as shown in Figure S2. Good correlations and quantitative agreement (within the combined uncertainties) between mass concentrations of total $PM_1$/main species in AMS and results from independent measurements (i.e., ion chromatography, scanning mobility particle sizer SMPS, and tapered element oscillating microbalance TEOM) support the reliability of our measurements (Figures S3–S5). The detection limits of main chemical components in AMS are listed in Table S1 and are typically far lower than the observed concentrations. All the reported mass concentrations from AMS in this study are based on ambient condition.

We used the procedures and software described in *Ulbrich et al*. [2009] to perform and applied positive matrix factorization (PMF) [*Paatero et al*., 2002] to the high-resolution OA mass spectral matrix for m/z 12–196 in W mode. The choice of the PMF solution is documented in the supporting information (Figures S6–S10 and Tables S2–S5). The elemental compositions (O/C; and hydrogen to carbon ratio = H/C) of total OA and of each PMF OA factor were calculated based on the updated ambient calibrations of *Canagaratna et al*. [2015]. The updated O/C ratios are ~20–30% and H/C ~5–10% higher than these calibrated with the previous Aiken method [*Aiken et al*., 2007; *Aiken et al*., 2008]. Those changes of O/C and H/C ratios between two methods are within the change range of elemetnal ratios in ambient OA reported by *Canagaratna et al*. [2015], which are 14–45% in O/C ratios with an average of 27% and 7–20% in H/C ratios with an average of 11%, and also similar to these studies from China (26%–31% in O/C ratios and 9%–12% in H/C ratios). For comparison with previous results, all the ambient related elemental ratio with original Aiken calibrations reported in other studies are multiplied by a ratio of 1.25 to the O/C and 1.09 to the H/C in this study. Thus, the cited O/C and H/C ratios in this study are 25% and 9% higher than their original reported values.

### 2.3. Other Instruments

The concentration of black carbon (BC) was measured with a multiangle absorption photometer (TSI Inc., USA) in summer and an Aethalometer (Magee Scientific, USA) in winter, respectively. The number size distributions of aerosols with mobility sizes between 15 and 650 nm were measured by a scanning mobility particle sizer (SMPS 3080, TSI Inc., USA). A commercial quadrupole-based proton transfer reaction-mass spectrometer (Ionicon Analytik, Austria) and a custom-built (by Peking University) online gas chromatograph-mass spectrometer (GC/MS) were used to measure multiple volatile organic compounds (VOCs) with time resolutions of 30 s and 30 min., respectively. The concentrations of gas phase $NO_2$/NO, $O_3$, and CO were measured with a time resolution of 1 min by the NO-$NO_2$-$NO_x$ analyzer (42i-TL, Thermofisher Scientific Inc., USA), $O_3$ analyzer (49i-TL, Thermofisher Scientific Inc., USA), and CO analyzer (48i-TL, Thermofisher Scientific Inc., USA), respectively.

## 3. Results and Discussion

### 3.1. Concentration and Chemical Composition of $PM_1$

Time series of mass concentrations of the main chemical species in $PM_1$ is shown in Figures 1 and 2. Quite different temporal variability of $PM_1$ was observed between the winter and summer studies, which should be mainly caused by the different meteorological conditions and emission source strengths in both seasons.

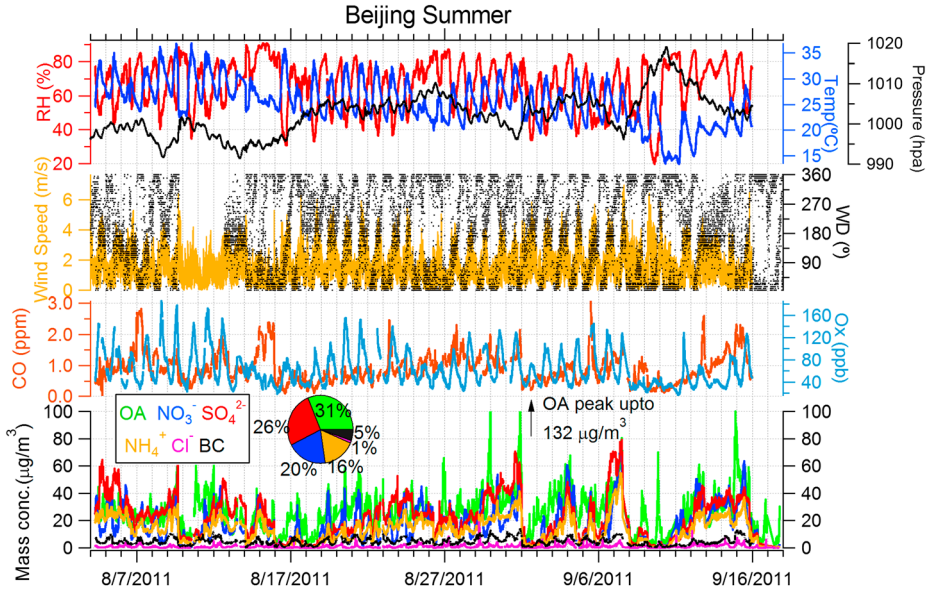


**Figure 1.** Time series of main species in $PM_1$, gas phase, and meteorology parameters (relative humidity, temperature, wind speed, and wind direction) in the summer of Beijing. The inset is the pie chart of average composition of $PM_1$ in this summer study.

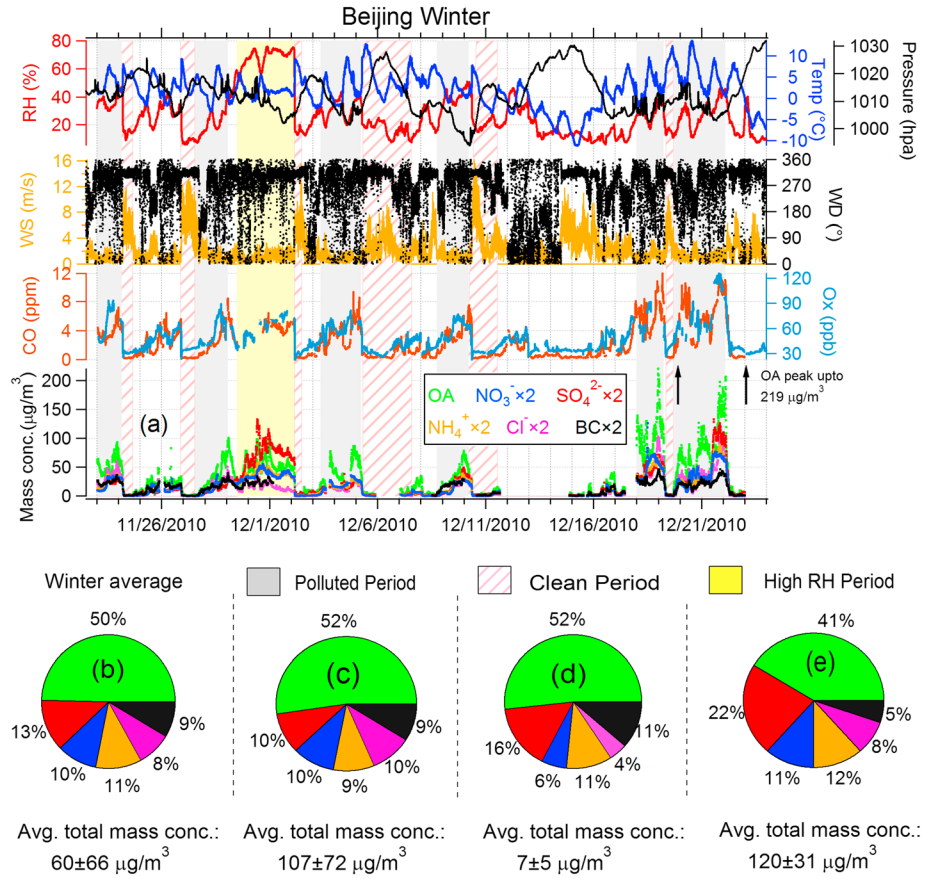


**Figure 2.** (a) Time series of main species in $PM_1$, gas phase, and meteorology parameters (relative humidity, temperature, wind speed, and wind direction) in the winter of Beijing. The average composition of $PM_1$ in the (b) whole winter campaign, (c) polluted, (d) clean, and (e) high RH periods in winter are also shown.

**Table 1.** Summary of Mass Concentrations of $PM_1$ Species and OA Components ($\mu g\,m^{-3}$), Mixing Ratios of Gas-Phase Pollutants, and Meteorological Parameters in the Winter and Summer Studies in Beijing

| | Beijing Summer (Average ± SD) | Beijing Winter (Average ± SD) | | |
|---|---|---|---|---|
| | | Clean Period | Polluted Period | Average |
| Total | 84. ± 47.4 | 6.6 ± 5.4 | 106.6 ± 71.5 | 60.0 ± 66.3 |
| OA | 26.4 ± 13.9 | 3.9 ± 2.8 | 58.7 ± 38.5 | 34.5 ± 35.2 |
| LO-OOA | 7.4 ± 5.1 | 0.2 ± 0.3 | 5.1 ± 4.5 | 4.3 ± 6.0 |
| MO-OOA | 9.7 ± 7.1 | 1.5 ± 0.8 | 10.1 ± 8.0 | 6.2 ± 6.5 |
| COA | 5.5 ± 6.1 | 0.9 ± 1.0 | 10.3 ± 9.2 | 6.7 ± 7.6 |
| HOA | 3.4 ± 3.0 | 0.4 ± 0.5 | 9.6 ± 5.9 | 4.7 ± 5.7 |
| CCOA | - | 0.6 ± 0.6 | 14.8 ± 17.0 | 8.2 ± 13.1 |
| BBOA | - | 0.1 ± 0.1 | 8.8 ± 11.9 | 4.1 ± 8.7 |
| Sulfate | 22.0 ± 15.3 | 1.2 ± 0.5 | 10.9 ± 9.8 | 8.7 ± 10.7 |
| Nitrate | 16.8 ± 13.1 | 0.5 ± 0.5 | 10.9 ± 7.7 | 6.8 ± 7.2 |
| Ammonium | 13.7 ± 9.3 | 0.8 ± 0.6 | 11.9 ± 8.3 | 7.7 ± 7.9 |
| Chloride | 1.0 ± 1.1 | 0.3 ± 0.5 | 10.8 ± 8.1 | 5.8 ± 7.0 |
| BC | 4.4 ± 1.9 | 0.9 ± 0.8 | 10.0 ± 4.1 | 6.0 ± 5.1 |
| CO (ppm) | 0.9 ± 0.5 | 0.5 ± 0.5 | 4.2 ± 2.4 | 2.6 ± 2.4 |
| NO (ppb) | 8.0 ± 14.5 | 8.4 ± 21.7 | 107.6 ± 55.5 | 65.9 ± 62.9 |
| $NO_2$ (ppb) | 35.6 ± 21.6 | 14.2 ± 10.9 | 58.8 ± 21.8 | 32.4 ± 27.1 |
| $SO_2$ (ppb) | 4.4 ± 2.6 | 6.8 ± 7.0 | 53.5 ± 26.8 | 87.3 ± 74.9 |
| $O_3$ (ppb) | 63.2 ± 30.6 | 20.2 ± 8.2 | 4.8 ± 4.3 | 9.5 ± 9.3 |
| Wind speed ($m\,s^{-1}$) | 1.0 ± 1.1 | 4.2 ± 2.3 | 1.2 ± 0.7 | 2.2 ± 2.0 |
| Temperature (°C) | 25.5 ± 4.2 | 4.7 ± 4.2 | 3.3 ± 3.2 | 2.7 ± 3.8 |
| RH (%) | 66.1 ± 14.1 | 16.7 ± 6.8 | 30.9 ± 9.1 | 29.1 ± 17.4 |
| Pressure (hPa) | 1002 ± 5.1 | 1008.6 ± 5.5 | 1016.1 ± 5.6 | 1012.5 ± 7.4 |

During the summer study, meteorological conditions were relatively stable (average wind speed = 1.0 ± 1.1 $m\,s^{-1}$; temperature = 25.5 ± 4.3°C; RH = 66.1 ± 4.3%) and daily repeated (Figure 1). The average $PM_1$ concentration in summer was 84 ± 47 $\mu g\,m^{-3}$ (Table 1). OA was the most abundant individual component (31%) in $PM_1$; however, the fraction of OA was lower than the total secondary inorganic aerosol (sulfate + nitrate + ammonium, SIA, 62%). The high SIA fraction, together with the substantial SOA contribution (see below), shows that secondary formation is the dominant source of $PM_1$ (82% of $PM_1$) in summer. Clear diurnal variations of main chemical species in $PM_1$ were observed in summer study (Figure S11). Diurnal pattern of sulfate peaks in the afternoon despite of the higher boundary layer height at this time, indicating the strong secondary formation properties of sulfate. The diurnal variations of nitrate and chloride show negative correlation with temperatures, suggesting that these two species are more controlled by the gas-particle partitioning process, consistent with previous results in Beijing [*Huang et al.*, 2010; *Sun et al.*, 2012].

In contrast to summer, the meteorological conditions in winter changed dramatically between different periods, leading to large variations of $PM_1$ mass concentrations from 0.6 to 368 $\mu g\,m^{-3}$, as well as large changes of other pollutants, e.g., CO (0.3 to 12 ppm) and $O_x$ ($O_x = O_3 + NO_2$; 30 to 120 ppb), as shown in Figure 2. Based on the patterns of $PM_1$, we divided the whole winter study into three typical periods.

*The first is polluted period.* (dark background in Figure 2). During this period, meteorological conditions were very stable usually with lower pressure and wind speed (1.2 $m\,s^{-1}$ on average), favoring the accumulation of pollutants. Taking the period from noon of 27–29 November as an example, all the mass concentrations of main chemical components in $PM_1$ increased very rapidly from a relatively clean background. The $PM_1$ mass increase rate was 4.2 $\mu g\,m^{-3}\,h^{-1}$ from the clean background (11 $\mu g\,m^{-3}$) to the highest peak (160 $\mu g\,m^{-3}$) in this period. On average, OA contributes 57% of $PM_1$ mass enhancement in this process, then followed by BC (11%) and chloride (10%). An even higher increase rate of $PM_1$ of 12 $\mu g\,m^{-3}\,h^{-1}$ was observed during 19–20 December. The frequent high mass increase rates (3–12 $\mu g\,m^{-3}\,h^{-1}$) of $PM_1$ indicate the haze appeared in the Beijing area quite fast (within several hours to 1 day), which should be a regional meteorology-controlled process [*Zheng et al.*, 2015]. The average $PM_1$ mass concentration during the whole polluted period was 106 ± 71 $\mu g\,m^{-3}$. The high fractions of BC (9% on average) in winter point out that $PM_1$ was strongly influenced by primary emissions sources in this period. The average diurnal variation of BC shows opposite diurnal profiles to that of wind speed, both in the winter and in summer studies (Figure S11), consistent with its primary sources.

The average chloride fraction (10%) during the polluted period is relative high as well. Submicron nonrefractory chloride in the aerosol phase can have primary and secondary sources, where the former can come from a direct emission from different sources (e.g., biomass burning, coal combustion, or waste incineration) and the latter is the result of chemical and physical processes leading to gas to aerosol conversion (e.g., $NH_4Cl$ partitioning) [*Wexler and Seinfeld*, 1990; *Andreae and Merlet*, 2001; *Watson et al*., 2001; *Salcedo et al*., 2006; *Li et al*., 2012; *Nuaaman et al*., 2015]. In the winter of Beijing, chloride show pronouncedly enhanced peak during night (Figure S11), which does not follow the expected time evolution for temperature-controlled partitioning of $NH_4Cl$. Together with the similarity of the chloride diurnal profile (Figure S11) to those of BBOA and CCOA ($R = 0.84$ and 0.68, respectively, Figure 5), this suggests that a large fraction of chloride in winter is due to primary emissions at night. Note that in summer, chloride (Figure S11) is much lower and does appear to follow an inverse temperature trend, suggesting a larger secondary semivolatile fraction.

In the winter study, good linear correlation of $Na^+$ ($R = 0.92$), $NaCl^+$ ($R = 0.82$), $K^+$($R = 0.92$ after 12 December), and $KCl^+$ ($R = 0.51$ after 12 December) ions detected in AMS with $Cl^+$ ion were found (Figures S12–S14), indicating part of chloride existed as KCl and NaCl in the aerosol phase. It is consistent with the direct emissions of KCl and NaCl species from biomass burning and coal combustion reported in the other field and emission studies [*Li et al*., 2003; *Doshi et al*., 2009; *Lewis et al*., 2009; *Yokelson et al*., 2009]. No enhanced $Na^+$, $NaCl^+$, and $KCl^+$ were found in the AMS measurement during the summer study. The measured $NH_4$ exceeded the $NH_4$ predicted assuming full neutralization of particulate anions nitrate and sulfate by an average factor of 1.2 (Figure S16). The excess $NH_4$ here (>20%) cannot be fully explained by the estimated organic influences (<10%, e.g., amine and organic nitrate in aerosol phase) to the measured inorganic species in AMS [*Docherty et al*., 2011], indicating that chloride measured in the winter study existed partially as $NH_4Cl$ in the aerosol phase. By comparing the excess $NH_4$ with $NH_4$ predicted with only anion chloride considered, we estimated >50% of chloride may exist as $NH_4Cl$ in the aerosol phase during the winter study (Figures S17 and S18). Direct emissions of $NH_4Cl$ or recondensation of $NH_4Cl$ from HCl(g) formed from reactions of coemitted KCl and NaCl with sulfuric acid ($H_2SO_4$) or nitric acid ($HNO_3$) are two possible pathways to explain the $NH_4Cl$ sources in biomass burning and coal combustion plumes [*Li et al*., 2003; *Yokelson et al*., 2009; *Levin et al*., 2010]. A detailed discussion on the chemical structure of chloride in the aerosol phase can be found in Text S4 in the supporting information.

*The second is clean period.* Polluted and clean periods usually alternate in the winter of Beijing. In clean periods, polluted air was usually advected away by clean air at high wind speeds of 5.2 m $s^{-1}$ on average from northern China (such as Inner Mongolia), Mongolia, or Siberia in Russia. The average $PM_1$ mass concentration in clean period was as low as $7 \pm 5\ \mu g\ m^{-3}$, 15 times less than the polluted period average ($106\ \mu g\ m^{-3}$). Figures 2c and 2d show that the average chemical composition did not change much between clean and polluted periods. We interpret this as being due to dilution effects that the aerosol mass concentrations in the clean air from northern part of China are so low that cannot substantially change the relative chemical composition of aerosols in polluted period but decrease the absolute ambient aerosol concentrations. New particle formation and growth was often observed during the clean periods, with expected important contributions from sulfuric acid [*Yue et al*., 2010; *Wang et al*., 2011]. As the image plot of particle number size distributions shown in Figure S19, we observed frequent new particle formation events in the clean periods in this study.

*The third is high RH period.* In this winter study, ambient RH was usually relative low, ranging from 16% to 30%. However, a relative high RH period (~2 days with RH > 60%) was observed (Figure 2e). In the winter study especially during this high RH period, sulfate closely correlated with RH with $R = 0.76$, implying the formation of sulfate during high RH period is probably strongly influenced by aqueous (or cloud) chemistry. Gas phase chemistry for sulfate formation, i.e., $OH + SO_2$, may be important during this period as well [*Zheng et al*., 2015]. Ammonium balance (measured $NH_4^+$/predicted $NH_4^+$) results show that the rapid increases in sulfate resulted in aerosols to be more acidic at the higher concentration levels in winter (Figure S19) [*Zhang et al*., 2007a], whereas the aerosol anions are neutralized by ammonium in summer.

Figure 3a shows the fractions of the main components in $PM_1$ as a function of $PM_1$ mass concentrations across the whole winter period. When the $PM_1$ concentration is above $50\ \mu g\ m^{-3}$, chloride fraction of $PM_1$ increases from 3% to 11% and BC fraction decreases from 17% to 5%; however, the OA fraction (~50%) and SIA fraction (~30%) stay quite stable, pointing to both contributions of primary emissions and secondary formation to high $PM_1$ concentration in this winter study. In summer (Figure 3b), the SIA fraction increases

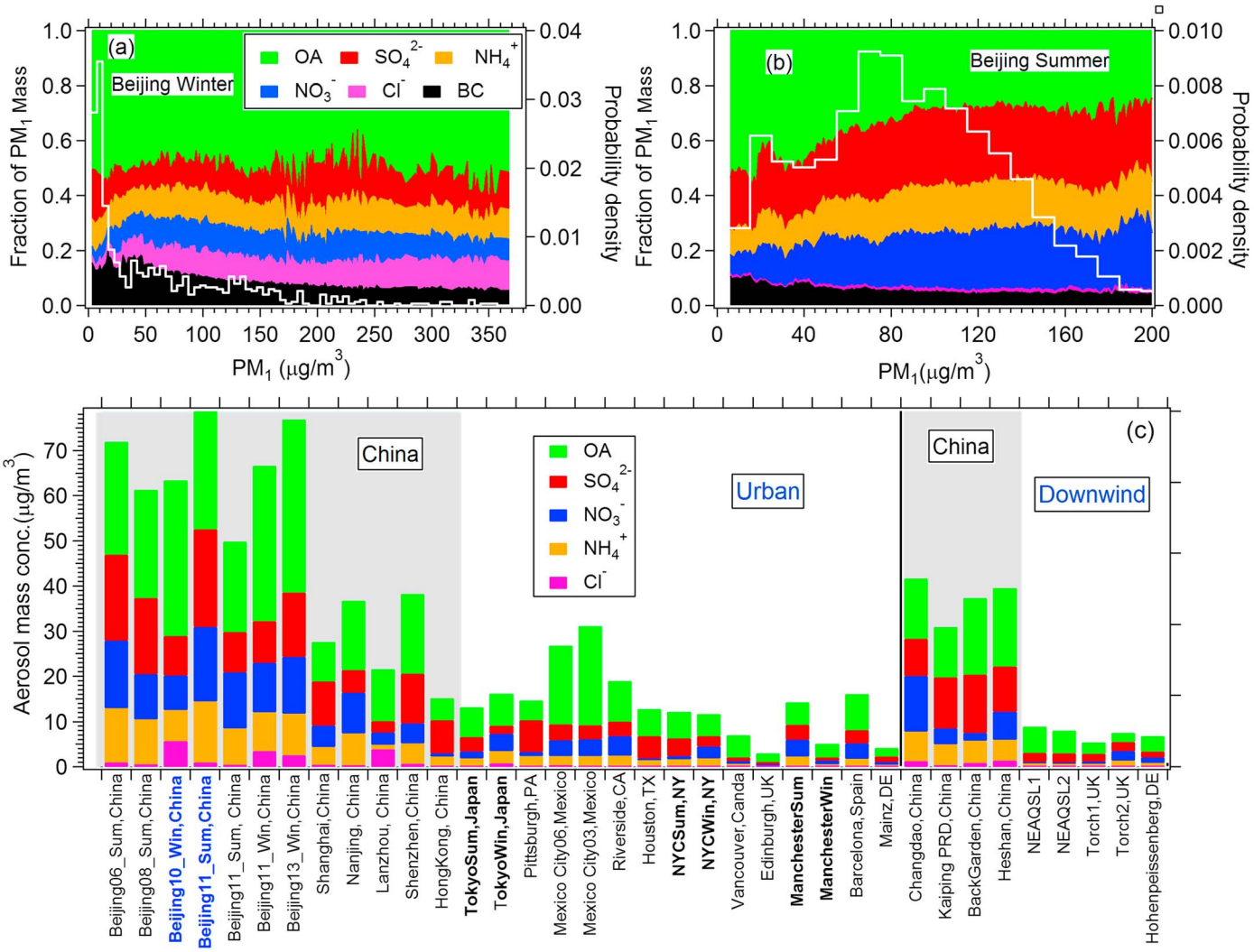


**Figure 3.** Variation of $PM_1$ compositions as a function of $PM_1$ mass concentrations in (a) winter and (b) summer. The probabilities of $PM_1$ mass in each study are also shown on the right axes. (c) The concentrations of nonrefractory $PM_1$ in various urban and downwind sites. Sites in China were labeled by the grey color in the background (detailed data are shown in Table S6 in the supporting information). Except summer/winter in Beijing, the other three urban summer/winter pairs are shown in black bold text. The non-China data set are obtained from *Zhang et al.* [2007b]. All the data sets and related references for Figure 3c can be found in Table S6.

substantially at high mass concentrations ($>50\,\mu g\,m^{-3}$), suggesting that the contribution from secondary formation is more important at higher $PM_1$ concentrations in this summer study.

Concentrations of nonrefractory $PM_1$ ($PM_1^{nr}$) measured by AMS in Beijing (summer and winter) and other various urban and downwind sites worldwide are summarized in Figure 3c. Average $PM_1^{nr}$ concentrations (60 to $80\,\mu g\,m^{-3}$) and chemical composition from 2006 to 2013 in Beijing were quite consistent and did not show a trend with year. Although severe haze was observed frequently in winter of Beijing, the average mass concentration of $PM_1^{nr}$ ($60–75\,\mu g\,m^{-3}$) in Beijing is still comparable to that ($48–80\,\mu g\,m^{-3}$) in summer because of the frequently occurring clean periods in winter. The high $PM_1^{nr}$ concentrations in Beijing are about twice those in other Chinese metropolitan areas such as Shanghai [*Huang et al.*, 2012], Shenzhen [*He et al.*, 2011], Lanzhou [*Xu et al.*, 2014], and Hong Kong [*Li et al.*, 2015] and 2–10 times higher than $PM_1$ mass concentrations measured in U.S. and European urban sites, including polluted regions such as Mexico City and the Los Angeles area. Meanwhile, the observed $PM_1^{nr}$ in the downwind sites of China also show much higher concentrations (3–8 times) than the results measured in similar sites in other countries [*Cubison et al.*, 2006; *Hings et al.*, 2007; *Takami et al.*, 2007]. Systematically higher $PM_1^{nr}$ concentrations in urban and suburban regions of China emphasize the heavily polluted air quality in China.

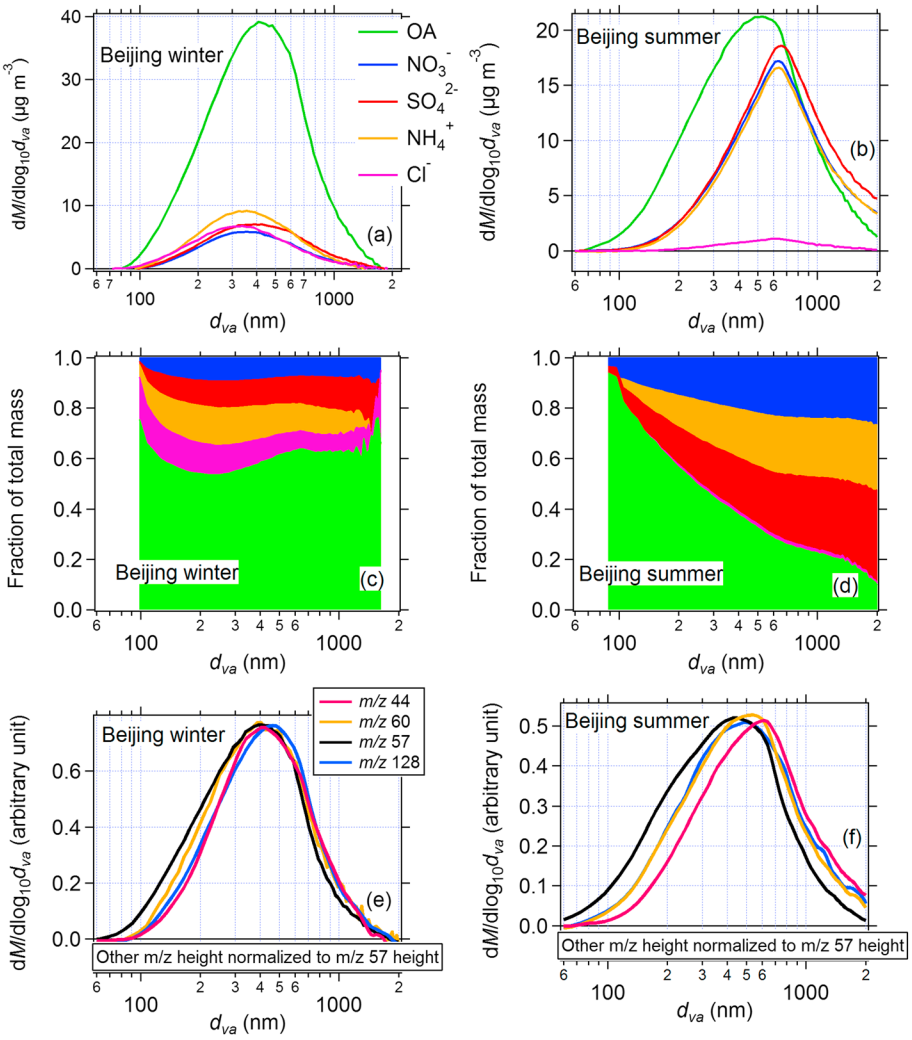


**Figure 4.** Averaged mass size distributions of OA, sulfate, nitrate, and ammonium and chloride in (a) winter and (b) summer. The fraction of chemical components as a function of particle sizes in (c) winter and (d) summer. Size distribution of selected m/z in (e) winter and (f) summer. To better distinguish the size distribution shapes, the size distributions of different ions in Figures 4e and 4f were multiplied by a factor to make their peak height consistently. The peak height of m/z 57 was used as a reference here. $CO_2^+$ is the main ion at m/z 44 ($CO_2^+/m44 = 84\%$ in winter and 92% in summer on average), $C_{10}H_8^+$ is the main ion at m/z 128 (win: 86%; sum: 60%) ; $C_2H_4O_2^+$ is the main ion at m/z 60 (win: 94%; sum: 60%); $C_4H_9^+$ and $C_3H_5O^+$ are two major ions at m/z 57 (win: 94% in total; sum: 96% in total).

### 3.2. Size Distributions of Main Species in $PM_1$

Average mass size distributions of AMS species (versus vacuum aerodynamic diameter, $d_{va}$, see *DeCarlo et al.* [2004]) in summer and winter are shown in Figures 4 and S21. Size distributions of SIA in summer all show very similar shapes and peak around 600 nm, suggesting internally mixed SIA [*Huang et al.*, 2010]. The average size distribution peaks (350 nm) of SIA in winter, mainly controlled by the polluted period, were systematically lower than those in summer. The differences of SIA size peaks may be caused by the lower photochemical activity in winter than summer, leading to a significant reduction of SIA production processes and consequently reduced particle growth rates. Higher new particle formation in winter also spreads the condensing mass onto more particles, leading to smaller average sizes. However, we found that average size distribution peaks of SIA (600–700 nm) in the high RH period of the winter study was systematically larger than those (300–400 nm) in clean and polluted periods (Figure S22), suggesting that the aqueous chemistry in the high RH period could lead to a faster particle growth rate of secondary species than photochemical activities or the aerosol is going through more cloud processing in this period, which also partially explain the high SIA (especially sulfate) concentrations measured in this high RH period [*Ge et al.*, 2012b].

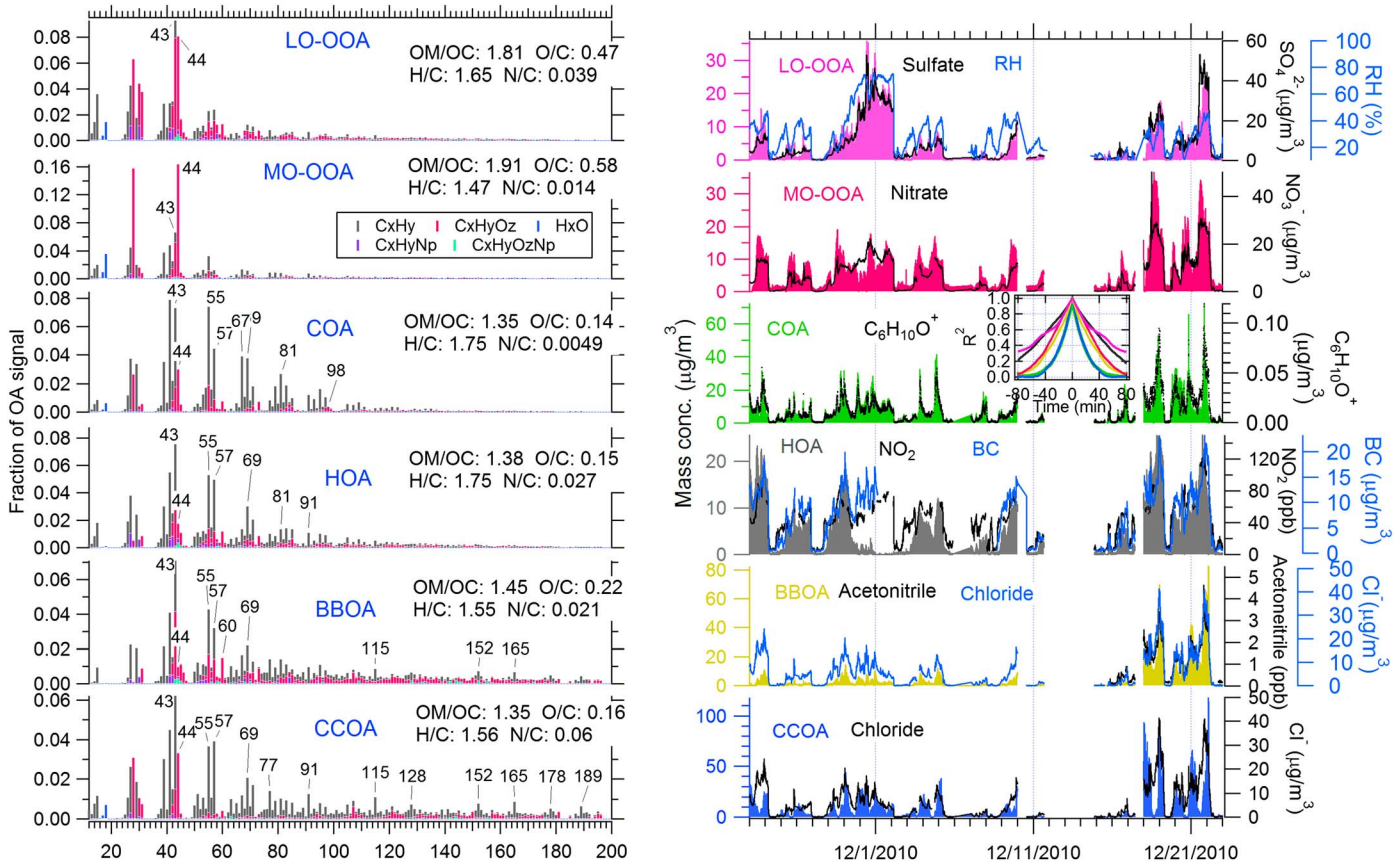


**Figure 5.** (left column) Spectra of different OA factors in winter; elemental ratios of each OA factor are also added. (right column) Time series of OA factors and other relevant species. The inset plot shows the autocorrelation of time series of different OA components (colors are those of the factor names in Figure 5 (right column)).

The average size distribution of OA in summer was much wider than that for SIA. The OA size distribution peaked around 500–600 nm and showed enhancements at small particle sizes (100–300 nm), as displayed in Figures 4b and 4d. The OA size enhancement in small mode is similar to other observations in the summer of Beijing, e.g., 2006 [*Sun et al.*, 2010], 2008 [*Huang et al.*, 2010], and some urban areas in North America [*Zhang et al.*, 2005a; *Aiken et al.*, 2009]. The enhancement of OA at smaller sizes may be associated with primary emissions from vehicle emissions, supported by the size distributions of m/z 57, which has strong contributions from primary emissions [*Zhang et al.*, 2005b] and is enhanced in the smaller sizes (Figure 4e). This contrasts with m/z 44, a marker of secondary OA and carboxylic acids [*Ng et al.*, 2011a; *Yatavelli et al.*, 2015]. The peak of OA in winter (400 nm) was smaller than in summer (500–600 nm). This may reflect not only the reduced secondary aerosol formation in winter but also the very high contributions from primary combustion sources (vehicle emissions, coal combustion, and biomass burning) in winter. For example, we observed ion m/z 57 from primary sources, m/z 60 substantially contributed by biomass burnings [*Cubison et al.*, 2011], and m/z 128, mainly composed of PAHs ions ($C_8H_{10}^+$) from coal combustion and BBOA [*Hu et al.*, 2013], tended to peak at the smaller size compared to oxygenated ion m/z 44. The percent of OA was above 50% across the whole size range in winter. However, SIA definitely dominated (>60%) the larger sizes (>400 nm) of $PM_1^{nr}$ in summer.

### 3.3. Primary OA Sources

The different chemical composition and size distributions of $PM_1$ between winter and summer imply different relative impacts of emission sources/formation pathways of OA in both seasons. In winter, six OA factors were resolved by the PMF method, as shown in Figure 5. They are more-oxidized oxygenated OA (MO-OOA; O/C = 0.58), less-oxidized oxygenated OA (LO-OOA; O/C = 0.47), cooking OA (COA; O/C = 0.14), biomass burning OA (BBOA; O/C = 0.22), coal combustion OA (CCOA; O/C = 0.16), and hydrocarbon-like OA (HOA, O/C = 0.15). In summer, four OA factors were found (Figure 6), which are MO-OOA (O/C = .82), LO-OOA

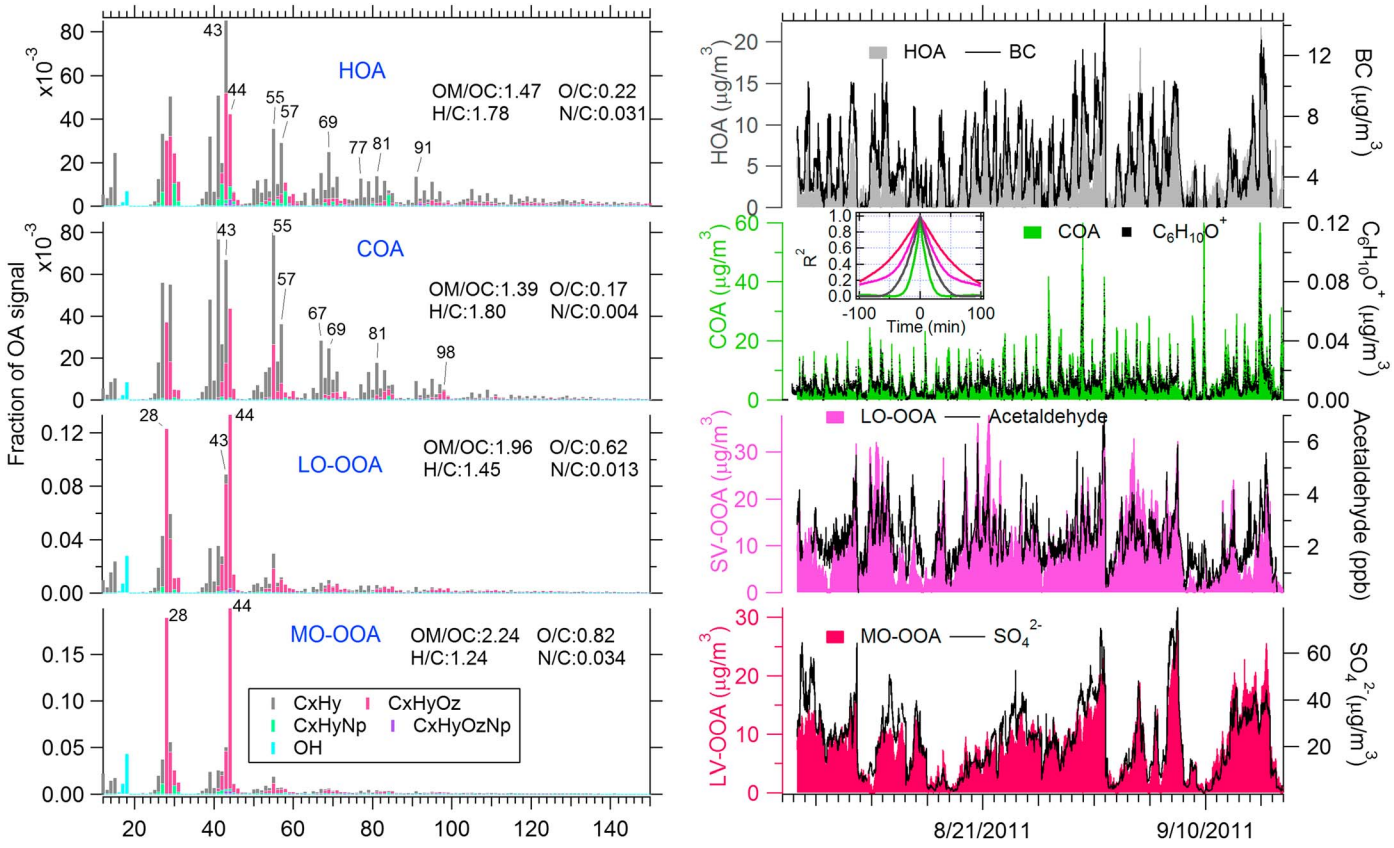


**Figure 6.** (left column) Spectra of different OA factors in summer; elemental ratios of each OA factor are also added. (right column) Time series of OA factors and other relevant species. The inset plot shows the autocorrelation of time series of different OA factors (colors are those of the factor names in Figure 6 (right column)).

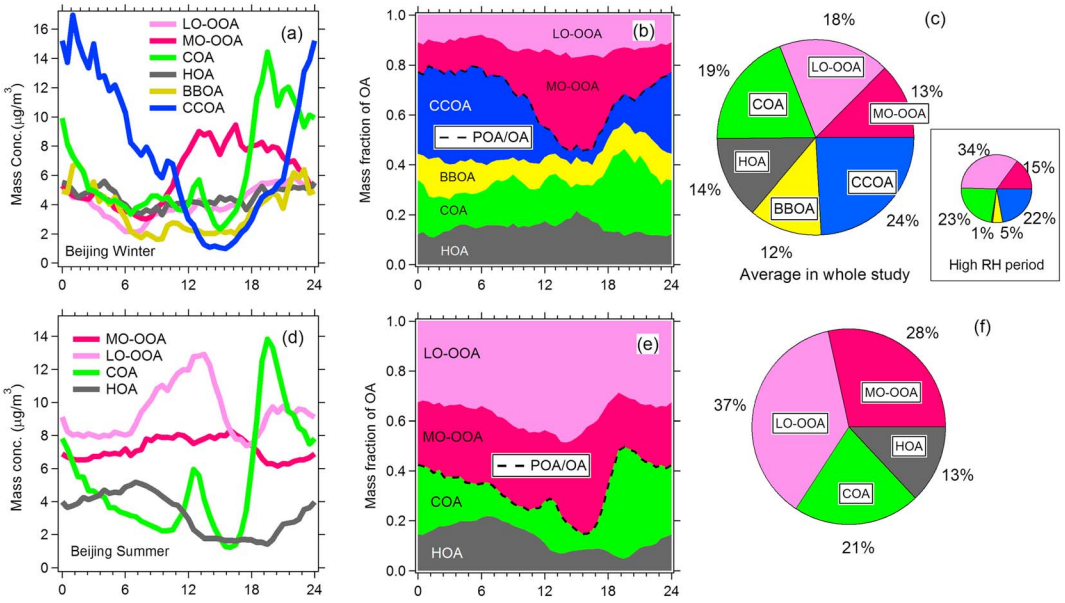


**Figure 7.** Diurnal variations of PMF factor mass concentrations in (a) winter and (d) summer; diurnal variations of PMF factor fractions of OA in (b) winter and (e) summer; average fractions of PMF factors in OA in (c) winter and (f) summer. The average fraction of PMF factors in OA during the high RH period of winter study is also shown.

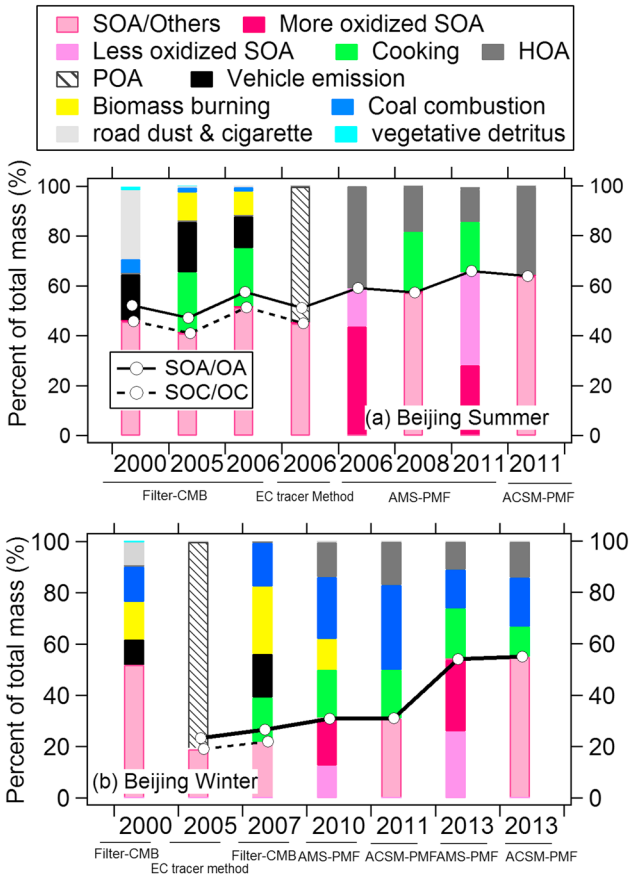


**Figure 8.** Comparisons of source apportionment of OA in the (a) summer and (b) winter studies of Beijing in recent years. The methods used in different studies are labeled in the bottom of *x* axis. Note that (1) the filter CMB method cannot resolve out SOA factor, so the fraction of OA named "others" in the CMB method is the sum of SOA plus unresolved/unknown OA, which represents the upper limits of the SOA fraction in OA. (2) We used 1.8 as a conversion factor to convert SOC to SOA and 1.4 for POC to POA for results from filter-CMB and EC-tracer method. These converting factor were obtained based on the OA/OC ratio of OOA and POA in this study (Figures 5 and 6). The data and corresponding references of other studies shown in Figure 8 can be found in Tables S8 and S9.

(O/C = 0.62), COA (O/C = 0.17), and HOA (O/C = 0.22). The O/C ratio in each factor was estimated by the updated method in *Canagaratna et al.* [2015]. Comparisons of O/C and H/C of each PMF factor between previous Aiken and updated Canagaratna methods can be found in Table S7. Detailed characteristics of different OA factors are discussed below.

### 3.3.1. Hydrocarbon-Like OA (HOA)

HOA was resolved in both summer and winter. Both HOA factors are substantially contributed by alkyl fragments ($C_nH_{2n+1}$ and $C_nH_{2n-1}$), as displayed in Figures 5 and 6, and show consistent peaks in both spectra (Figure S23). The change of O/C ratios between previous and updated calibration methods in both HOA factors resolved in this study (22% and 25% in winter and summer) is similar to the change of HOA (24%–31%) reported in *Canagaratna et al.* [2015]. The updated O/C ratios in both HOA (0.15 and 0.22 in winter and summer) are similar to values of HOA (0.05–0.25) obtained in other studies [*Jimenez et al.*, 2009; *Huang et al.*, 2010; *Morgan et al.*, 2010; *Ng et al.*, 2011b], considering applying the updated calibration (a factor of 1.25 from HOA in the winter study, Table S7) to the published results. Good correlation between HOA and primary emission tracers (i.e., BC and $NO_x$) suggests that HOA in Beijing is mainly contributed by vehicle emissions. *Wang et al.* [2009] reported that vehicle emissions can account for 12–16% of organic carbon in the summer (2006) and winter (2005) of Beijing-based molecular-level OA source apportionment, which are similar to the HOA fractions (13% in summer and 14% in winter) in our study. The enhancements in the diurnal variations of HOA around 7:00–9:00 are consistent with the rush hour of Beijing traffic (Figure 7) [*Lin et al.*, 2009; *Huang et al.*, 2010].

### 3.3.2. Coal Combustion OA (CCOA)

Coal combustion is one of the main energy sources in China and is used extensively for domestic heating in northern China [*Zhang et al.*, 2008]. Coal consumption in China increases yearly and accounted for ~70% of total energy consumption from 2005 to 2011 in China, with use in power plants year round and for domestic heating during cold periods only [*Zhang et al.*, 2012]. Coal combustion OA was only resolved in the winter study, indicating that this CCOA factor is dominated by domestic burning with higher OA emission factors [*Chen et al.*, 2005; *Zhang et al.*, 2008]. In addition to alkyl fragments ($C_nH^+_{2n+1}$ and $C_nH^+_{2n-1}$), typical of POA ions from fossil fuel combustion, the spectrum of CCOA also showed pronounced peaks of polycyclic aromatic hydrocarbons (PAHs) ions (e.g., $C_{10}H_8^+$ naphthalene and $C_{14}H_{10}^+$ anthracene), consistent with the high PAHs fraction in OA (>50%) from domestic coal combustion [*Xu et al.*, 2006]. The CCOA spectrum in the winter study is also similar to CCOA spectrum resolved in Changdao, China [*Hu et al.*, 2013]. Compared to the H/C in other primary OA (1.8–2.0) [*Jimenez et al.*, 2009; *Mohr et al.*, 2009], H/C in CCOA (1.56) is lower. The OA/OC and O/C ratios in CCOA were 1.35 and 0.16, respectively.

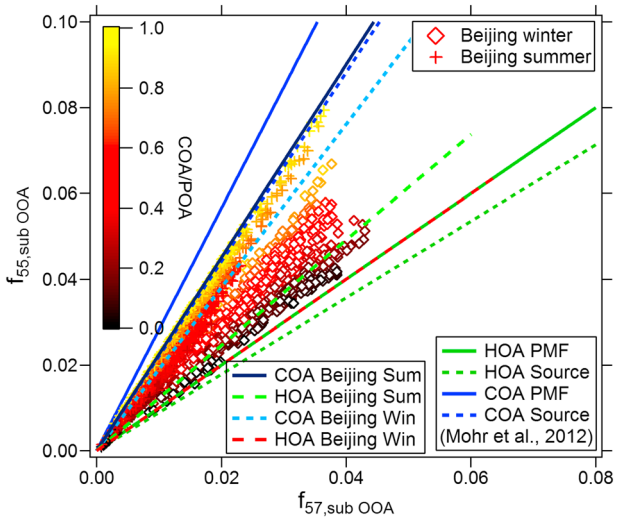


**Figure 9.** Scatterplots between $f_{55}$ versus $f_{57}$ in Beijing. The $f_{55}$ versus $f_{57}$ ratios of "HOA PMF" and "COA PMF" represent average $f_{55}$ versus $f_{57}$ values from a small subset of summarized HOA and COA PMF factors in *Mohr et al.* [2012]. The $f_{55}$ versus $f_{57}$ ratios of "HOA source" and "COA sources" represent $f_{55}$ versus $f_{57}$ values averaged from several lab source studies reported in *Mohr et al.* [2012]. $f_{55,\ sub\ OOA} = (m/z\ 55 - m/z55_{MO-OOA} - m/z55_{LO-OOA})/OA$; $f_{57,\ sub\ OOA} = (m/z\ 57 - m/z57_{MO-OOA} - m/z57_{LO-OOA})/OA$.

CCOA accounted for 24% of total OA on average, within the range of 10–33% reported in other studies in the winter of Beijing (Figure 8). CCOA shows clear diurnal variations with low mass concentrations (down to 2 $\mu g\,m^{-3}$) in daytime and high (16 $\mu g\,m^{-3}$) at night, corresponding to 3.4% and 40% of total OA, respectively (Figures 7a and 7b). The high abundance (40%) of CCOA in total OA points to strong coal combustion emissions in the evening and night in Beijing, which is consistent with the residential heating periods.

### 3.3.3. Cooking OA (COA)

COA resolved by AMS OA spectra are widely reported in urban areas with high population densities [*He et al.*, 2010; *Huang et al.*, 2010; *Mohr et al.*, 2012]. In the year of 2011, the population in Beijing reached 20 million with over 70,000 restaurants [*News*, 2011]. In this study, cooking OA was resolved in both winter and summer seasons (Figures 5 and 6). The spectra of COA in our study contained many alkyl fragments and a certain amount of oxygen-containing ions, consistent with aliphatic acids (e.g., linoleic acid and palmitic acid) in the cooking oils or fat of the meat reported in other studies [*He et al.*, 2004; *Zhao et al.*, 2007; *Mohr et al.*, 2009; *He et al.*, 2010]. *Allan et al.* [2010] also reported the similarity between the spectra of PMF-resolved COA and cooking oil, suggesting that the oil vaporized from cooking process may significantly contribute the COA mass resolved by AMS. The O/C of COA in summer and winter were 0.17 and 0.14, and OA/OC ratios were 1.39 and 1.35, respectively.

*Mohr et al.* [2012] found the ratio between m/z 55 ($C_4H_7^+ + C_3H_3O^+$) and m/z 57 ($C_4H_9^+ + C_3H_5O^+$) is distinctly higher (2.2–2.8) than the ratios (0.9–1.1) in other noncooking POA components. COA resolved in Beijing had consistently high m/z 55 versus m/z 57 ratios of 2.25 (summer) and 1.9 (winter) as well (Figure 9). In the ambient bulk OA data, the ratio between $f_{55}$ (= m/z 55/OA) and $f_{57}$ (= m/z 57/OA) in Beijing increased proportionally as the COA fractions of OA increased in both studies (Figure 9). Similar COA fraction dependence trend was also observed in the ratio between hydrocarbon ions ($C_4H_7^+$ versus $C_4H_9^+$ ) and oxygenated ions ($C_3H_3O^+$ versus $C_3H_5O^+$ ) in m/z 55 and m/z 57 (Figure S24). In some ambient measurements, $C_6H_{10}O^+$ (m/z 98) in AMS OA spectra was reported to be a tracer of COA [*Sun et al.*, 2011]. We checked through all correlations between time series of organic ions in AMS and COA resolved in this study and also found that $C_6H_{10}O^+$ ion correlates best with COA ($R = 0.94$) and thus is its best internal tracer. Around 65% of this ion signal in summer was contributed by COA, with other contributions from LO-OOA and MO-OOA (Figure S25). In winter, biomass burning OA also can contribute to $C_6H_{10}O^+$ background (Figure S26). The relative abundance of $C_6H_{10}O^+$ in COA is around 0.3–0.4%.

In this study, the most pronounced feature of COA is its clearly enhanced diurnal peaks around noon (12:00–13:00) and late evening (19:00–20:00), consistent with common lunch and dinner times. During these meal times, COA can account for 45% and 35% of total OA on average or ~25% of total $PM_1$, signifying the importance of controlling cooking sources as strategy to reduce aerosol mass concentrations in Beijing or other urban areas.

Time series of species concentrations can be analyzed using an autocorrelation plot. In these plots, correlation of each factor with itself is calculated for various time offsets [e.g., *Hayes et al.*, 2013]. Components with high-frequency fluctuations (i.e., spikes in time) in their time series will have a steep autocorrelation profile and vice versa. This plot is shown in the insets of Figures 5 and 6. In the autocorrelation plot, COA has the steepest profile

**Table 2.** Mass Concentrations of Cooking OA and Its Fractions of OA in Beijing and Other Cities

| Observation Site | Sampling Period | Percentage of OA (%) | Mass Concentrations ($\mu g\ m^{-3}$) | References |
|---|---|---|---|---|
| Beijing, China | 2010 Winter | 19 | 6.6 | This study |
| Beijing, China | 2011 Summer | 21 | 5.5 | This study |
| Beijing, China | 2008 Summer | 24 | 5.8 | *Huang et al.* [2010] |
| Beijing, China | 2011 Winter | 19 | 6.6 | *Sun et al.* [2013] |
| Beijing, China | 2013 Winter | 13 | 4.8 | *Sun et al.* [2014] |
| Beijing, China | 2013 Winter | 20 | 8.9 | *Zhang et al.* [2014] |
| **Average Beijing Studies** | | 19.3 ± 3.6 | 6.4 ± 1.4 | |
| Lanzhou, China | 2012 Jul to Aug | 24 | 2.8 | *Xu et al.* [2014] |
| London, UK | 2006 Oct | 22 | - | *Allan et al.* [2010] |
| London,UK | 2007 Oct to Nov | 30 | - | *Allan et al.* [2010] |
| Manchester,UK | 2007 Jan | 19 | - | *Allan et al.* [2010] |
| Paris | 2009 Jul | 15 | 0.33 | *Crippa et al.* [2013] |
| Barcelona, Spain | 2009 Mar | 17 | 1.5 | *Mohr et al.* [2012] |
| Zurich, Switzerland | 2005 Summer | 6.5 | 0.43 | *Lanz et al.* [2008] |
| Los Angeles, USA | 2010 May to Jun | 17 | 1.2 | *Hayes et al.* [2013] |
| New York, USA | 2009 Summer | 16 | 1.0 | *Sun et al.* [2011] |
| Fresno, USA | 2010 Jan | 19 | 1.5 | *Ge et al.* [2012a] |
| **Average western cities** | | 17.9 ± 6.2 | 1.0 ± 0.5 | |

and thus has the most local character of all OA components in both seasons. Coal combustion OA in winter also show similar peak width as COA in autocorrelation plot, indicating that the CCOA is likely from local sources as well.

Overall, COA was 21% of total OA in summer and 19% in winter on average, consistent with previous results (13–24%) listed in Table 2, indicating that cooking is a stable contributor to OA in Beijing. By combining our results and the published results, we find that the average COA fraction (19 ± 3% of OA) in Beijing is comparable with COA fractions (18 ± 6%) in western cities, whereas the average COA mass concentration in Beijing ($6 \pm 1\ \mu g\ m^{-3}$ versus $1 \pm 0.5\ \mu g\ m^{-3}$) is much higher.

*Huang et al.* [2014] and *Zhang et al.* [2015b] used radiocarbon measurements to quantify the nonfossil fraction of OA in the winter (January 2013) of Beijing as 37–52% at different degree of polluted days. However, they assigned nonfossil SOA and BBOA to be the main sources of nonfossil organic carbon, neglecting the contribution of cooking sources. Based on the source apportionment results in our study and multiple other studies in Figure 8, COA can contribute substantially (13–24%) to total OA and specifically account for 45–50% of nonfossil POA matter in this study. Thus, the contribution of cooking to nonfossil OC in Beijing should not be omitted. The total nonfossil primary organic carbon (cooking + biomass burning, not including SOA) in this study can account for 27% and 33% of total OC in the summer and winter, respectively.

#### 3.3.4. Biomass Burning OA (BBOA)

BBOA was only identified in winter as well. *Wang et al.* [2009] showed that wood combustion is the main source of biomass burning (90%) and that the straw combustion contribution is relatively small (10%) in the winter of Beijing. We found good agreement on time series of BBOA and biomass burning tracers acetonitrile ($R = 0.91$) [*Yuan et al.*, 2010] and chloride ($R = 0.84$) [*Andreae and Merlet*, 2001], as shown in Table S5. m/z 60 in AMS OA spectra is a tracer of BBOA [*Alfarra et al.*, 2007; *Lee et al.*, 2010; *Cubison et al.*, 2011]. Analysis on HR OA spectra showed that m/z 60 was dominated by $C_2H_4O_2^+$, which is mainly enhanced by biomass-burning tracer levoglucosan and related species (mannosan, galactosan, etc.) [*Cubison et al.*, 2011]. Scatterplots of $f_{44}$ versus $f_{60}$ in summer are totally outside of empirical triangle area of biomass burning plumes and within the nonbiomass burning influenced background areas (Figure S27a), consistent with negligible biomass burning contributions to the OA in summer of Beijing. We observed higher $f_{60}$ and lower $f_{44}$ in winter (toward the center of triangle area of biomass burning plumes) as BBOA increased its relative importance in total OA (Figure S27b). The $f_{44}$ and $f_{60}$ of BBOA (0.01 versus 0.015) from the winter study are also within the triangle area and show similar range to the other BBOA PMF factors or these from biomass burning chamber studies. The other non-BBOA POA factors in winter show less $f_{60}$ ($\leq$0.01) than BBOA (0.015).

BBOA had an O/C ratio of 0.22, thought to be contributed by oxygenated species from biomass burning [*Aiken et al.*, 2010]. BBOA accounts for 12% of total OA on average in winter. The diurnal variations of BBOA were similar to those of CCOA, i.e., higher in the evening and night and lower during daytime.

**Table 3.** Summary of Elemental Ratios and Other Key Parameters in This Study

| | Beijing Winter | Beijing Summer |
|---|---|---|
| OA/OC ratio | 1.58 ± 0.1 | 1.91 ± 0.1 |
| O/C ratio | 0.32 ± 0.07 | 0.56 ± 0.1 |
| H/C ratio | 1.65 ± 0.04 | 1.61 ± 0.06 |
| N/C | $1.6\times10^{-2}\pm0.4\times10^{-2}$ | $2.0\times10^{-2}\pm0.5\times10^{-2}$ |
| Total POA/ΔCO ($\mu g\,m^{-3}\,ppm^{-1}$) | 11 | 16 |
| Noncooking POA/ΔCO[a] ($\mu g\,m^{-3}\,ppm^{-1}$) | 9 | 6 |
| $OOA/O_x$ ($\mu g\,m^{-3}\,ppb^{-1}$) | 0.49 | 0.22-1.2 |
| $k_{OH}$ of OA aging ($cm^3\,molecule^{-1}\,s^{-1}$) | - | $4.1\times10^{-12}$ |

[a]Cooking OA was excluded in POA/CO calculation.

However, BBOA represented a relatively constant fraction of total OA in diurnal profiles, indicating biomass burning in winter is likely a more regional than urban phenomenon in this area [*Duan et al.*, 2004; *Wang et al.*, 2009]. This conclusion is also supported by the broader $R^2$ peak width of BBOA than those from CCOA and COA in the autocorrelation plot (inset in Figure 5).

### 3.3.5. POA/CO Ratios

In summary, total POA accounts for 69% and 34% of OA in winter and summer, respectively. The average fraction of total primary species (including POA, BC, and chloride) in $PM_1$ is 58% and 18%, respectively. Several studies show that POA has good correlation with primary emitted species CO in the urban area [*Turpin and Huntzicker*, 1995; *de Gouw and Jimenez*, 2009]. Even though different sources emit POA and CO in different ratios, the sources are very finely intermixed spatially in an urban area, and thus, the emission ratio for the whole urban area can be studied. This emission ratio can be used to estimate POA contributions to the global OA budget. *De Gouw and Jimenez* [2009] reported that POA/ΔCO ratios (above background levels of CO) in urban areas can range from 3 to 15 $\mu g\,m^{-3}\,ppm^{-1}$. For comparisons, ratios between POA/ΔCO (above background levels of CO) in the winter and summer of Beijing, as well as Changdao island located in downwind of the North China Plain are also investigated by regressing POA and ΔCO. CO background (100 ppb in summer and 140 ppb in winter) was determined by the lowest CO concentration observed in the summer and winter study, respectively, as shown in Figure S28. Finally, emission ratios of POA versus ΔCO under ambient condition are 11 $\mu g\,m^{-3}\,ppm^{-1}$ in Beijing winter, 16 $\mu g\,m^{-3}\,ppm^{-1}$ in summer, and 13 $\mu g\,m^{-3}\,ppm^{-1}$ in Changdao island (Table 3 and Figure S29), which is comparable to the values reported in the eastern U.S. (9 $\mu g\,m^{-3}\,ppm^{-1}$) [*de Gouw and Jimenez*, 2009], Los Angeles (6.4–13 $\mu g\,m^{-3}\,ppm^{-1}$) [*Hayes et al.*, 2013], and Tokyo (11–14 $\mu g\,m^{-3}\,ppm^{-1}$) [*Takegawa et al.*, 2006]. Cooking sources emit much less CO than the other combustion OA, and a much higher COA/ΔCO ratio than other combustion OA/ΔCO was observed (e.g., OA/ΔCO of with high COA abundance in OA is a factor of 2 higher than with HOA in Los Angeles) [*Hayes et al.*, 2013]. If we exclude COA in the POA/ΔCO calculations, the emission ratios of POA versus ΔCO in winter and summer are 9 and 6 $\mu g\,m^{-3}\,ppm^{-1}$, respectively.

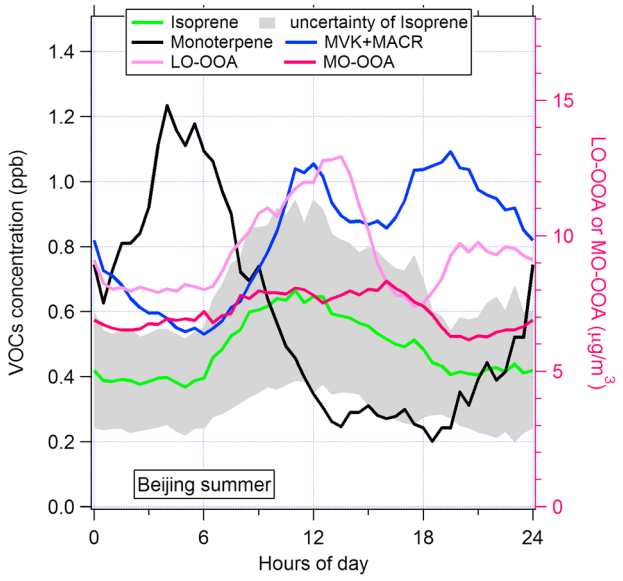


**Figure 10.** Diurnal variations of VOCs species isoprene, monoterpene, and isoprene oxidation product MVK + MACK (left axis), together with LO-OOA and MO-OOA (right axis) in the summer study of Beijing.

## 3.4. Oxygenated OA Sources

### 3.4.1. LO-OOA and MO-OOA

In the summer study, two SOA factors (MO-OOA and LO-OOA) were resolved. Comparisons between time series of MO-OOA and LO-OOA factors with other gas, aerosol species, and meteorological parameters are listed in Tables S3 and

S5. Both OOA factors are very similar to the spectra of other OOA factors resolved in other cities [*Mohr et al*., 2012; *Hayes et al*., 2013; *Zhang et al*., 2014]. MO-OOA in summer was relatively aged with high O/C of 0.82 and OA/OC of 2.24 (Figure 5), similar to values of aged SOA reported in remote regional areas [*Turpin and Lim*, 2001; *Hu et al*., 2012; *Canagaratna et al*., 2015]. The time series of MO-OOA correlated well ($R = 0.90$) with sulfate (Figure 6), which is produced over regional scales [*Canagaratna et al*., 2007]. A similar good correlation between OOA and sulfate was observed in previous Beijing summer studies [*Huang et al*., 2010; *Sun et al*., 2010] and in western urban areas [*Aiken et al*., 2009; *Mohr et al*., 2012; *Hayes et al*., 2013].

LO-OOA resolved in summer was less aged with an O/C of 0.62 and OA/OC of 1.96. LO-OOA correlates well with VOC photochemical products (e.g., isoprene oxidation product methyl vinyl ketone (MVK) + Methacrolein (MACR), $R = 0.61$ acetaldehyde, $R = 0.76$, and acetone, $R = 0.73$), as shown in Figures 6 and 10. The major sources of MVK + MACR (lifetime = approximately half a day) and acetaldehyde (lifetime = ~1 day) should be from photochemical oxidation in the atmosphere [*Jacob et al*., 2002; *Millet et al*., 2010; *Slowik et al*., 2010]. The good correlation between LO-OOA and these oxidized VOCs indicates that LO-OOA was a more freshly formed SOA by photochemical activities [*Slowik et al*., 2010], consistent with its lower O/C than MO-OOA. In addition, despite the much deeper boundary layer in daytime, the diurnal profile of LO-OOA showed a pronounced peak at noon (Figure 7), supporting the association of LO-OOA as a strong local/regional photochemical product. The average isoprene and MVK + MACR concentrations in Beijing study are $0.49 \pm 0.2$ and $0.85 \pm 0.5$ ppb, respectively. The good correlation ($R = 0.61$) and similar diurnal variation (Figure 10) between MVK + MACR and LO-OOA imply that isoprene oxidation might contribute to SOA formation in the summer of Beijing. However, the absolute biogenic contribution to total SOA formation in Beijing should be small, based on the low relative concentrations of biogenic VOCs to OA and the calculated values of $k_{OH}$ in total OA, which will be discussed in section 3.7. LO-OOA and MO-OOA account for 28.4% and 37.3% of total OA on average. High SOA fraction (66%) of OA is consistent with strong photochemical activity in summer.

In winter, two SOA factors were also resolved, as shown in Figure 5. We also name them LO-OOA and MO-OOA, although their sources and properties may be different from the components of the same name identified in the summer study, since the PMF analyses were performed independently. LO-OOA in winter showed good correlation with sulfate ($R = 0.93$) and RH ($R = 0.79$). The covariations between LO-OOA with sulfate and RH suggest that formation of LO-OOA may be driven by aqueous or cloud chemistry in regional air masses [*Lee et al*., 2012; *Zheng et al*., 2014]. The liquid water content (LWC) in the aerosol phase during the winter study (especially during high RH periods, LWC $> 100\ \mu g\ m^{-3}$) were similar to those observed in the summer study (mainly from 50 to $200\ \mu g\ m^{-3}$) (Figure S30), the latter of which is suggested to be contributed by aqueous reactions (see section 3.4.3). The comparable LWC levels between winter and summer studies indicate condensed phase water in aerosol during some high RH periods of the winter study should not be the limiting factor to initialize the aqueous phase reaction, compared to Beijing summer. Although the RH value was measured at ground site, the consistence that higher RH (>50%) corresponds to higher sulfate fraction in total sulfur, also known as sulfate oxidation ratio, indicates that RH here can roughly reflect the RH history that the aerosols have experienced (Figure S31).

As discussed earlier, the aerosol in winter was more acidic at high sulfate concentrations. It is unclear whether acid-catalyzed or enhanced reactions in wet aerosols contribute to LO-OOA formation in winter. Based on box model results which simulated urban SOA formation under high $NO_x$ conditions, *McNeill et al*. [2012] found that SOA formed through aqueous reactions is insensitive to the pH and tends to increase with RH. Here we examine the effect of aerosol acidity influences by using ammonium balance ratio to color code the scatterplots of LO-OOA versus $O_x$ (Figure S32). The slope of latter was usually used as diagnostic tools to examine the photochemical oxidation of SOA [*Herndon et al*., 2008]. The results show that LO-OOA/$O_x$ slopes does not have a dependency on acidity of aerosol. Thus, the acidity of aerosol might not play an important role to the LO-OOA formation in winter, consistent with the box model results [*McNeill et al*., 2012].

The autocorrelation plot (Figure 5, inset) shows a narrower width for MO-OOA versus LO-OOA, suggesting MO-OOA in winter is more local than LO-OOA. This conclusion is also supported by the diurnal variation of MO-OOA, with a pronounced peak in the afternoon despite the expanded boundary layer, implying that the MO-OOA in winter may be formed through photochemical processes in the daytime. The diurnal MO-OOA fractions of total OA was also more enhanced than the constant fraction of LO-OOA. MO-OOA showed good correlation ($R = 0.86$) with nitrate, whose formation has an important contribution from gas-particle partitioning and

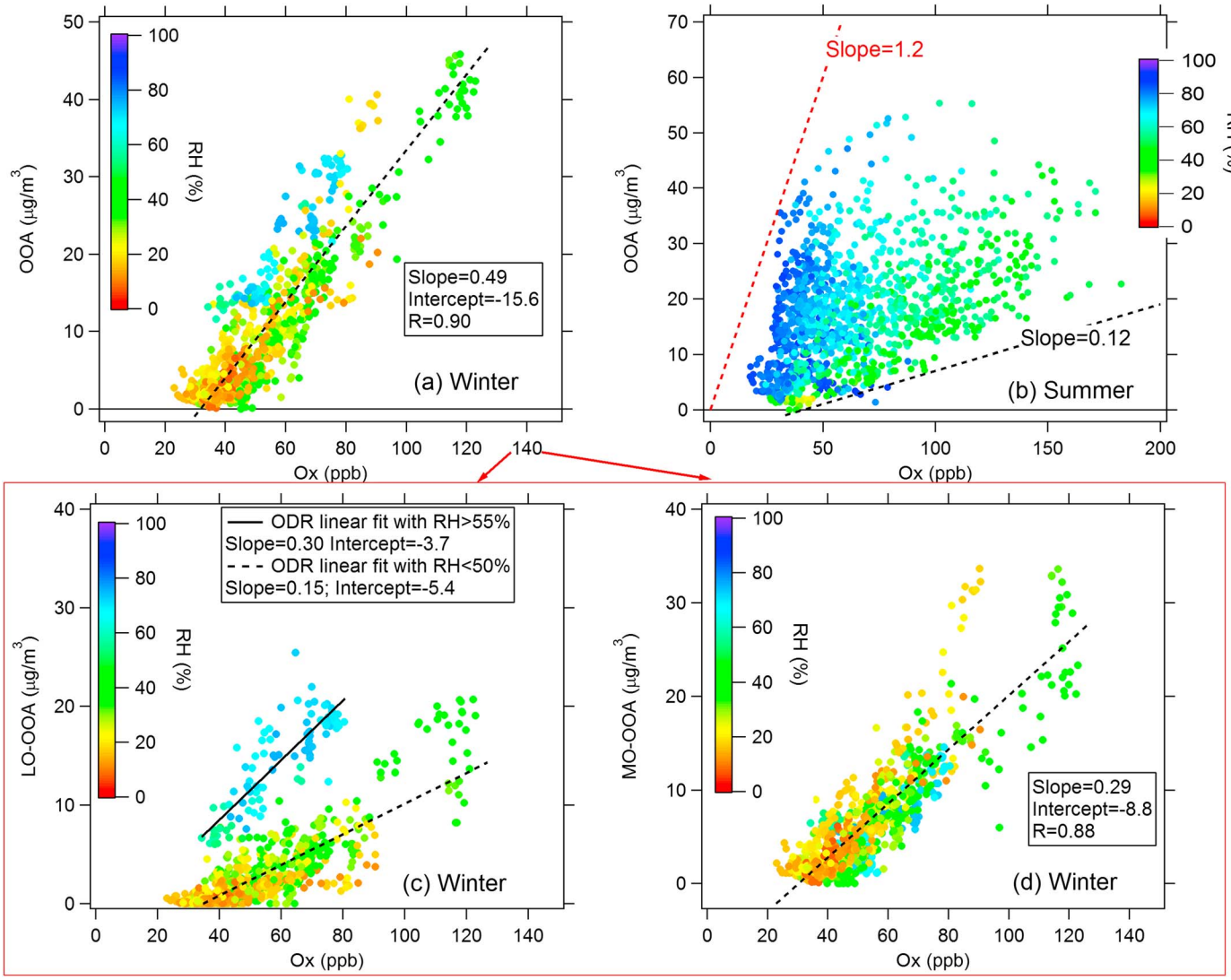


**Figure 11.** Scatterplots of OOA versus $O_x$ in the (a) winter and (b) summer studies, as well as (c) LO-OOA versus $O_x$ and (d) MO-OOA versus $O_x$ in the winter study. All scatterplots are color coded by ambient RH.

photochemical formations. The total average fraction of SOA (MO-OOA + LO-OOA) in winter is around 31% but can be as high as 50% in the high RH period with aqueous chemistry contributions (Figure 7).

The scatterplots of four OOA spectra in summer and winter are shown in Figure S33. In summary, the LO-OOA (O/C = 0.62) in summer study and MO-OOA (O/C = 0.58) in the winter study are more related with photochemistry and have similar oxidation level. A better correlation of spectra ($R = 0.97$) between LO-OOA in summer and MO-OOA in winter was also found. The MO-OOA (O/C = 0.82) in summer study and LO-OOA (O/C = 0.47) in the winter study, both of which are supposed to go through more regional process and with partial aqueous chemistry contributions, show a large difference (a factor of 1.7) in oxidation levels, consistent with the stronger oxidation capacity of air in the summer and weaker in the winter study.

### 3.4.2. Comparison With Other SOA Source Apportionments

Besides this study, several other studies have been published to investigate the OA sources in the Beijing area in the last several years. By comparing our source apportionment results with the literatures' results (Figure 8), we found that SOA composes 45–67% of the total OA in the summer of Beijing, indicating that secondary sources are consistently the most important source of OA concentrations in this season. Taking into account SIA, secondary sources can explain three quarters (82% in this study) of $PM_1$ in summer [*Zheng et al.*, 2005; *Lin et al.*, 2009; *Wang et al.*, 2009; *Sun et al.*, 2013]. SOA fractions of total OA in Beijing winter varied between

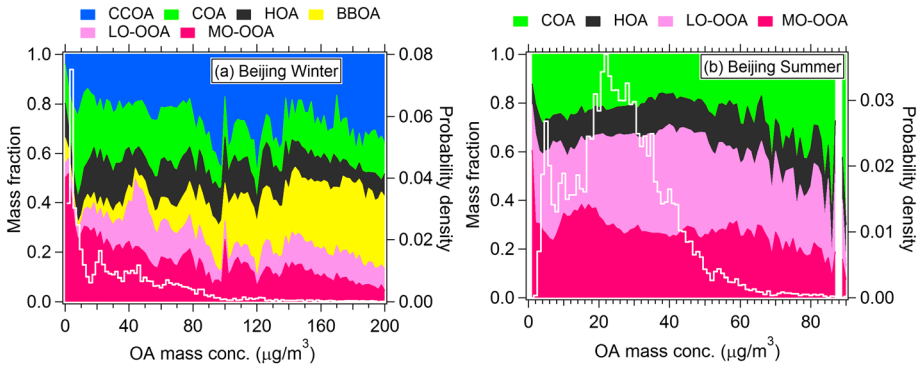


**Figure 12.** PMF factor fractions of OA as a function of total OA mass concentrations in Beijing (a) winter and (b) summer.

23 and 33% from 2000 to 2011, indicating that POA dominates but SOA is still significant in winter. However, in recent studies, *Sun et al*. [2014], *Zhang et al*. [2014], and *Huang et al*. [2014] showed similar conclusions based on independent measurements at the same winter period (January 2013) in Beijing where SOA may account for more than 50% of total OA during hazy days. This is consistent with our results: on one of the haze period (high RH period: 30 November to 2 December) with relative high RH (70%), we also observed 50% of OA is SOA. Thus, we conclude that the OA in the winter of Beijing has a larger contribution from POA. However, in the occasional high RH periods, SOA from aqueous chemistry leads to high sulfate and SOA formation and also can contribute substantially to haze period.

### 3.4.3. OOA Versus $O_x$

Regression slopes between OOA and $O_x$ in photochemically processed urban emissions provide a metric to investigate the relative efficiency of SOA versus $O_3$ formation during photochemical oxidation [*Herndon et al*., 2008; *Wood et al*., 2010; *Hayes et al*., 2013].

Scatterplots of OOA versus $O_x$ in summer and winter are shown in Figure 11 and Table 3. We found strong correlation between OOA and $O_x$ in winter with a regression slope of 0.49 $\mu g\,m^{-3}\,ppb^{-1}$ under ambient condition and 0.486 in standard condition (temperature = 273.15 K and 1 atm.). This slope is about three times higher than the ratios obtained in the other strong anthropogenic emissions-influenced urban areas, such as Pasadena, CA, of 0.15 $\mu g\,m^{-3}\,ppb^{-1}$ [*Hayes et al*., 2013], Riverside, CA, of 0.14 $\mu g\,m^{-3}\,ppb^{-1}$ [*Docherty et al*., 2011], Houston, TX, of typical 0.03 $\mu g\,m^{-3}\,ppb^{-1}$ [*Wood et al*., 2010], Mexico City of 0.16 $\mu g\,m^{-3}\,ppb^{-1}$ [*Herndon et al*., 2008], Tokyo of 0.19 $\mu g\,m^{-3}\,ppb^{-1}$ [*Morino et al*., 2014], and Paris of 0.14 $\mu g\,m^{-3}\,ppb^{-1}$ [*Zhang et al*., 2015a], indicating that SOA versus $O_3$ formation chemistry in winter is quite different with that in other cities. Note that the low ratio in Houston is thought to be due to very strong emissions of small alkenes which form $O_3$ efficiently but not SOA [*Wood et al*., 2010]. Several reasons may explain the higher $OOA/O_x$ ratios observed in the winter study.

*The Differences of VOCs Precursor Between Beijing and Other Studies*. Although the emission ratio (VOCs versus CO) in Beijing is very similar to the U.S. cities for short-chain VOCs species ($< C_{10}$) [*Yuan et al*., 2012], a higher abundance of semivolatile VOCs (e.g., PAHs and long-chain alkanes with $C > 10$) is likely in the winter of Beijing, because of the strong primary sources of biomass burning, coal combustions, and vehicle emissions [*Presto et al*., 2009; *Ortega et al*., 2013]. However, semivolatile species were not measured in this study or in any other studies in Beijing, to the best of our knowledge. Changdao island is located in the downwind of the North China Plain and has both coal combustion and vehicle emission contributions to OA as Beijing winter study [*Hu et al*., 2013]. *Yuan et al*. [2013] estimated that the potential SOA formation from semivolatile species can be 2–3 times higher than that from all measured short-chain VOCs at Changdao island. In addition, the average temperature in the winter study is 2.7 ± 3.8°C that is much lower than the 16–27°C in other studies (Houston, Pasadena, and Mexico City) discussed above. The lower temperatures in winter of Beijing also facilitate the partitioning of semivolatile oxidized species into particle phase which may help to close the gap of $OOA/O_x$ between the winter study in Beijing and other studies in western cities.

*Extra Aqueous SOA Formation in the Particle Phase*. RH was used to color code the scatterplots of OOA versus $O_x$, together with MO-OOA and LO-OOA versus $O_x$ (Figure 11). Results show that $LO\text{-}OOA/O_x$ ratios tend to be higher

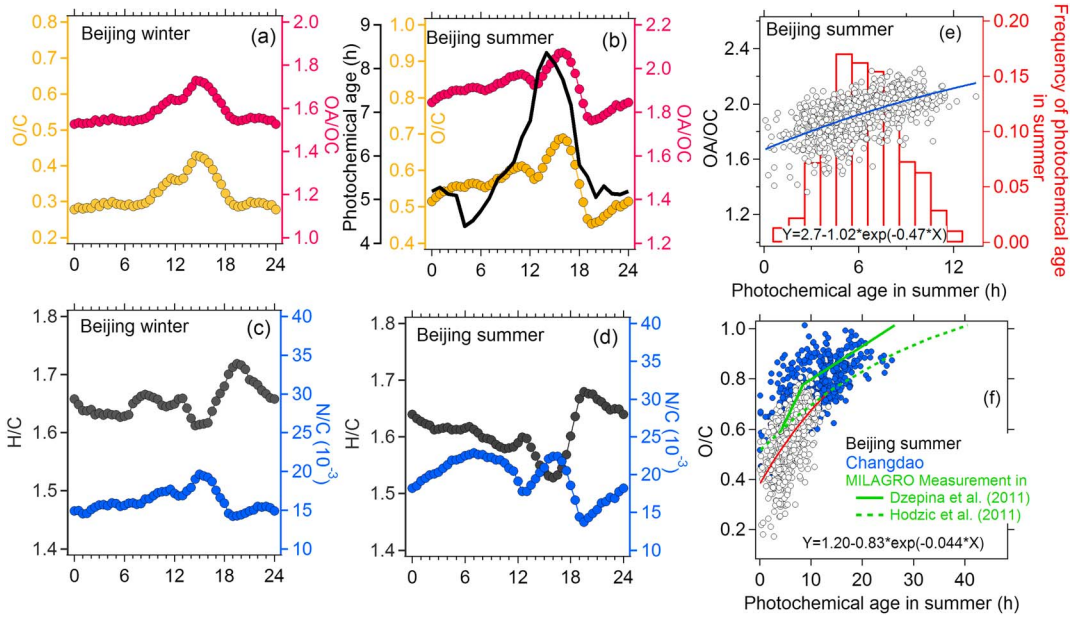


**Figure 13.** Diurnal variation profiles of elemental ratios in OA in the (a, c) winter and (b, d) summer studies of Beijing; (e) OA/OC and (f) O/C as a function of photochemical age in the summer study of Beijing. The histogram of photochemical age in summer study is also shown on the right axis of Figure 13e. For comparison, a factor of 1.25 was multiplied to the O/C in both studies in MILAGRO (Megacity Initiative-Local And Global Research Observations) field measurement [*Dzepina et al.*, 2011; *Hodzic and Jimenez*, 2011] for converting the O/C based on previous calibration [*Aiken et al.*, 2007] to updated new correction [*Canagaratna et al.*, 2015]. The curve in *Dzepina et al.* [2011] is the measured O/C results and in *Hozidic et al.* [2011] is the model fitting result.

during the high RH period (>50%), suggesting that SOA formed by aqueous chemistry can increase the ratio compared to gas-phase photochemistry (together with $O_x$ formation). The MO-OOA/$O_x$ ratios do not show obvious dependent trend on RH (Figure 11d), which is reasonable since MO-OOA was suggested to be mainly from photochemical processes. Note that $O_x$ formation may also be reduced under cloudy conditions, affecting the ratio.

In contrast to winter, the ratio between OOA and $O_x$ spans a very wide range in summer (Figure 11b). High RH (from 20 to 91%, 66 ± 14% on average) was typical in summer. The ratios between OOA and $O_x$ increase gradually with RH, from 0.12 to 1.2 $\mu g\, m^{-3}\, ppb^{-1}$. Although the diurnal variation of RH is coincidently opposite to the diurnal profile of $O_x$, a factor of 2–3 of RH variation ratio in summer cannot fully explain the large variation ratio of 10 in OOA/$O_x$, indicating that the secondary formation through aqueous reaction is likely a potential contributor to SOA formation in summer as well.

### 3.5. Source Contributions to OA Enhancement

OA in Beijing varied between 1.7 to 132 $\mu g\, m^{-3}$ in summer and 0.2 to 220 $\mu g\, m^{-3}$ in winter. Figure 12 shows the relative importance of the OA sources at different OA concentrations. In summer, OOA was the dominant component (50–80%) across the whole range of OA mass variations. In contrast, in winter there is a clear trend with OOA being more important at lower OA and the POA sources becoming more dominant at the higher OA concentrations. Biomass burning and coal combustion OA are enhanced during the periods with the highest concentrations. BBOA and CCOA can explain 57% of total OA at high OA mass concentrations (>100 $\mu g\, m^{-3}$). Total POA/OA fraction increases at a rough rate of 0.25% per $\mu g\, m^{-3}$. The health effect of coal combustion OA and biomass burning OA, which has been found causing respiratory and allergic diseases [*Kleinerman et al.*, 2002; *Lundstedt et al.*, 2007], should be seriously considered for the high abundance of toxic PAHs in these two OA sources.

### 3.6. Diurnal Variation of OA Elemental Composition

OA/OC and O/C can be used as surrogates to represent the oxidation level of OA. More aged OA tends to have higher OA/OC and O/C [*Aiken et al.*, 2008; *Jimenez et al.*, 2009]. OA/OC ratios are usually in the range of 1.4–1.8 for urban area and 2.0–2.5 for oxidized OA aerosol in remote areas [*Turpin and Lim*, 2001; *Aiken*

*et al*., 2008; *Hu et al*., 2012]. The average OA/OC and O/C in winter (1.58 ± 0.1 and 0.32 ± 0.07) were consistently lower values than these in summer (1.91 ± 0.1 and 0.56 ± 0.1), consistent with stronger photochemical activity and SOA contribution in summer versus dominance of primary emissions in winter. The average H/C ratios in summer and winter were 1.61 ± 0.06 and 1.65 ± 0.04, respectively.

The oxidation states of OA in summer and winter showed similar diurnal variations (Figure 13). O/C and OA/OC started to increase in the morning and then peaked in the afternoon. Both parameters stayed about constant between 6:00–8:00 A.M., which may be caused by the vehicle emissions in the morning rush hours in both seasons. The decrease of OA/OC and O/C around noon (12:00–13:00) and late evening (19:00–20:00) was consistent with the cooking emission peaks in both seasons shown in Figure 7. OA/OC and O/C in summer increased after the late evening till dawn, while the oxidiation levels in winter were more stable during night. The different trends may be due to continuing SOA formation or OA aging (with oxidant $O_3$ or $NO_3$) at the night of summer. In contrast, continuing primary emissions of coal combustion OA in the night of winter may counteract any additional SOA formation or aging, thus resulting in a relative constant OA/OC and O/C ratios in winter. Elemental H in OA mainly comes from the fragments of alkyl ions [*Aiken et al*., 2008]. With the oxidation process of OA, the alkyl ions were replaced with oxidized ions containing O elements [*Aiken et al*., 2008; *Heald et al*., 2010]. Hence, the diurnal variations of H/C ratio show the opposite trend to O/C ratio (Figures 13c and 13d).

### 3.7. Estimation of $k_{OH}$ for OA Aging

The OA/OC and O/C ratios as a function of photochemical age in summer are shown in Figures 13e and 13f. Data from Changdao island were also added as a reference [*Hu et al*., 2013]. The photochemical age in summer was estimated from the ratio of VOCs species benzene and *m*,*p*-xylene based on their different reaction rates with OH radicals, further leading to different lifetimes in the atmosphere. Detailed information on photochemical age (OH exposure) is given in *Yuan et al*. [2013]. An average OH concentration of $1.5 \times 10^6$ molecule $cm^{-3}$ was used to calculate photochemical age (0–12 h) in the summer study. OA/OC increased with photochemical age from 1.4 to 1.8 at lower ages (0–2 h) to 1.8–2.2 at higher photochemical ages (10–12 h). Photochemical age in summer is lower than the values obtained in Changdao island, consistent with the fact that the sampling site is an urban site, closer to the emissions sources than at downwind site (Figure 13f). The evolution of O/C with photochemical age in Changdao and Beijing is also comparable to what is observed in Mexico City [*Dzepina et al*., 2011; *Hodzic and Jimenez*, 2011], consistent with the anthropogenic precursors dominated in both areas.

Empirical rate constants of anthropogenically dominated OA aging with OH radical ($k_{OH}$) are a useful parameter for regional and global SOA modeling work and for comparison across locations [*Dzepina et al*., 2011; *Hodzic and Jimenez*, 2011]. If we assume the SOA formation and aging can be represented as a first-order process proportional to OH radical concentration, then the $k_{OH}$ of OA aging can be estimated by fitting the scatterplot of OA/OC (or O/C) versus photochemical age (Figure 13f) following equation: $OA/OC = A - B \times \exp(C \times age)$. The $k_{OH}$ can be estimated by the fitted parameter $C$ in the equation divided by the average OH concentration [*DeCarlo et al*., 2010]. $k_{OH}$ estimated in summer is $4.1 \times 10^{-12}$ $cm^3$ $molecule^{-1}$ $s^{-1}$. This value is slightly smaller than the value ($5.2 \times 10^{-12}$ $cm^3$ $molecule^{-1}$ $s^{-1}$) obtained at Changdao island and within the range of $k_{OH}$ (3–$12.5 \times 10^{-12}$ $cm^3$ $molecule^{-1}$ $s^{-1}$) of SOA formation applied in other anthropogenic influenced areas, and far below $k_{OH}$ values (>$50 \times 10^{-12}$ $cm^3$ $molecule^{-1}$ $s^{-1}$) for biogenic VOCs oxidation (Figure S34) [*Hodzic and Jimenez*, 2011; *Spracklen et al*., 2011].

In this study, we did not estimate the photochemical age in winter due to two reasons: (1) online GC/MS data were not available for the winter study. (2) Primary emission ratios of VOCs (e.g., xylene versus ethane or benzene versus toluene) used to calculate photochemical age change diurnally in winter. According to our source apportionment results, primary emission ratios of VOCs in winter are more dominated by vehicle emission during the day and coal combustion in the night. The changing primary emission ratios of VOCs across the day lead to extra uncertainties to the calculation of photochemical age in winter. Thus, it is unlikely that photochemical age can be calculated correctly and accurately in the winter studies of Beijing even with VOCs data available.

## 4. Conclusions

Intensive campaigns in the winter and summer were carried out in the years 2010 and 2011 to examine the seasonal characteristics of $PM_1$ in urban area of Beijing. We used a commercial HR-ToF-AMS together with other

fast-response online instruments. Aerosol composition, sources, and aging process in both seasons were investigated, which showed distinctive influences on $PM_1$ because of the different intensities of emission sources (anthropogenic activities) and formation pathways mainly caused by varied meteorological conditions.

$PM_1$ in Beijing area in recent years are relatively stable (60–84 $\mu g\,m^{-3}$) and show consistent chemical composition. $PM_1$ in Beijing is around 2–10 times higher than in European and U.S. cities, signifying the severe polluted air condition in Beijing. $PM_1$ in summer was quite stable with clear diurnal variation of each species. However, dramatic changes were observed in winter (0.6 $\mu g\,m^{-3}$ to 368 $\mu g\,m^{-3}$) due to the alternation of clean periods dominated by advection of clean air from northern areas and polluted periods with stagnant meteorological conditions. Occasional high RH periods happened, which likely facilitate aqueous or cloud chemistry in the atmosphere to contribute to the $PM_1$ increase.

In summer, although OA is the most abundant component (31%) of $PM_1$, the fraction of SIA can account for 62% of $PM_1$. In total, 82% of $PM_1$ on average was secondary, where 20% is due to SOA in addition to SIA. In winter, OA is the main component of $PM_1$ (57%), and the average SIA fraction is only 29%. The high average fraction (58%) of primary species in $PM_1$ including POA (39%), black carbon (BC, 9%), and chloride (10%) indicates primary emissions played a more important role in our winter study. However, during the high RH period in the winter study, SIA can reach 45% of total $PM_1$ concentration and half of OA is SOA. The high secondary fraction of $PM_1$ (SIA + SOA = 65%) potentially come from aqueous reaction or cloud processing in the atmosphere. Thus, both primary species (e.g., polluted period) and secondary species (e.g., RH period) could be major contributor to extreme high $PM_1$ concentrations ($>100\,\mu g\,m^{-3}$) in winter time of Beijing.

We summarized the source apportionment in different studies in recent years of Beijing and found 45–67% of OA in summer and 22–50% of OA in winter can be composed of SOA in Beijing. For the POA, we estimate that 45% of POA in winter and 61% in summer are from nonfossil sources, mainly cooking OA (COA) in both seasons and biomass burning OA (BBOA, 12% of OA) in winter. Some studies on Beijing have neglected cooking as nonfossil carbon sources; however, multiple independent measurements show that 13–24% of OA are from cooking in different seasons of Beijing, suggesting that COA should not be omitted as nonfossil OA. The fossil sources of POA include hydrocarbon-like OA (HOA, 14% and 13% of OA in winter and summer, respectively) from vehicle emissions in both seasons and coal combustion OA (CCOA) in winter. CCOA peaking during the evening and night, together with BBOA, which is more regional than CCOA, were the two main contributors (57% of OA) for the highest OA concentrations ($>100\,\mu g\,m^{-3}$) in winter, emphasizing the importance of controlling heating sources to improve the winter air quality in Beijing. The health effect of CCOA and BBOA should be seriously considered for the high abundance of toxic PAHs in these two factors. POA/$\Delta$CO ratios in winter and summer are 11 and 16 $\mu g\,m^{-3}\,ppm^{-1}$, respectively.

Average O/C ratios in summer and winter are $0.56 \pm 0.1$ and $0.32 \pm 0.07$, respectively. O/C ratio in OA is an important parameter to represent the aging state of aerosol plumes. By regressing the scatterplot of O/C versus photochemical age, an average $k_{OH}$ value of OA aging in summer of Beijing is calculated to be around $4.1 \times 10^{-12}\,cm^3\,molecule^{-1}\,s^{-1}$, which is in the range of $k_{OH}$ values ($3–12.5 \times 10^{-12}\,cm^3\,molecule^{-1}\,s^{-1}$) of anthropogenic VOCs reported in U.S. and Mexico City and far below $k_{OH}$ values ($>50 \times 10^{-12}\,cm^3\,molecule^{-1}\,s^{-1}$) for biogenic VOCs oxidation.

**Acknowledgments**

This work was supported by the Strategic Priority Research Program of the Chinese Academy of Sciences (XDB05010500), National Basic Research Program, China Ministry of Science and Technology (2013CB228503), National Natural Science Foundation of China (21190052; 91544214), and the China Ministry of Environmental Protection's Special Funds for Scientific Research on Public Welfare (20130916). J.L.J. was supported by NSF AGS-1360834. The data presented in this study are available from the authors upon request (minhu@pku.edu.cn).

## References

Aiken, A. C., P. F. DeCarlo, and J. L. Jimenez (2007), Elemental analysis of organic species with electron ionization high-resolution mass spectrometry, *Anal. Chem.*, *79*(21), 8350–8358.

Aiken, A. C., et al. (2008), O/C and OM/OC ratios of primary, secondary, and ambient organic aerosols with high-resolution time-of-flight aerosol mass spectrometry, *Environ. Sci. Technol.*, *42*(12), 4478–4485.

Aiken, A. C., et al. (2009), Mexico City aerosol analysis during MILAGRO using high resolution aerosol mass spectrometry at the urban supersite (T0)—Part 1: Fine particle composition and organic source apportionment, *Atmos. Chem. Phys.*, *9*(17), 6633–6653.

Aiken, A. C., et al. (2010), Mexico city aerosol analysis during MILAGRO using high resolution aerosol mass spectrometry at the urban supersite (T0)—Part 2: Analysis of the biomass burning contribution and the non-fossil carbon fraction, *Atmos. Chem. Phys.*, *10*(12), 5315–5341.

Alfarra, M. R., A. S. H. Prevot, S. Szidat, J. Sandradewi, S. Weimer, V. A. Lanz, D. Schreiber, M. Mohr, and U. Baltensperger (2007), Identification of the mass spectral signature of organic aerosols from wood burning emissions, *Environ. Sci. Technol.*, *41*(16), 5770–5777.

Allan, J. D., P. I. Williams, W. T. Morgan, C. L. Martin, M. J. Flynn, J. Lee, E. Nemitz, G. J. Phillips, M. W. Gallagher, and H. Coe (2010), Contributions from transport, solid fuel burning and cooking to primary organic aerosols in two UK cities, *Atmos. Chem. Phys.*, *10*(2), 647–668.

Andreae, M. O., and P. Merlet (2001), Emission of trace gases and aerosols from biomass burning, *Global Biogeochem. Cycles*, *15*(4), 955–966, doi:10.1029/2000GB001382.

Canagaratna, M. R., et al. (2007), Chemical and microphysical characterization of ambient aerosols with the aerodyne aerosol mass spectrometer, *Mass Spectrom. Rev.*, *26*(2), 185–222.

Canagaratna, M. R., et al. (2015), Elemental ratio measurements of organic compounds using aerosol mass spectrometry: Characterization, improved calibration, and implications, *Atmos. Chem. Phys.*, *15*(1), 253–272.
Chan, C. Y., X. D. Xu, Y. S. Li, K. H. Wong, G. A. Ding, L. Y. Chan, and X. H. Cheng (2005), Characteristics of vertical profiles and sources of PM2.5, PM10 and carbonaceous species in Beijing, *Atmos. Environ.*, *39*(28), 5113–5124.
Chen, Y., G. Sheng, X. Bi, Y. Feng, B. Mai, and J. Fu (2005), Emission factors for carbonaceous particles and polycyclic aromatic hydrocarbons from residential coal combustion in China, *Environ. Sci. Technol.*, *39*(6), 1861–1867.
Crippa, M., et al. (2013), Identification of marine and continental aerosol sources in Paris using high resolution aerosol mass spectrometry, *J. Geophys. Res. Atmos.*, *118*, 1950–1963, doi:10.1002/jgrd.50151.
Cubison, M. J., et al. (2006), The characterisation of pollution aerosol in a changing photochemical environment, *Atmos. Chem. Phys.*, *6*, 5573–5588.
Cubison, M. J., et al. (2011), Effects of aging on organic aerosol from open biomass burning smoke in aircraft and laboratory studies, *Atmos. Chem. Phys.*, *11*(23), 12,049–12,064.
de Gouw, J., and J. L. Jimenez (2009), Organic aerosols in the Earth's atmosphere, *Environ. Sci. Technol.*, *43*(20), 7614–7618.
DeCarlo, P. F., J. G. Slowik, D. R. Worsnop, P. Davidovits, and J. L. Jimenez (2004), Particle morphology and density characterization by combined mobility and aerodynamic diameter measurements. Part 1: Theory, *Aerosol Sci. Technol.*, *38*(12), 1185–1205.
DeCarlo, P. F., et al. (2006), Field-deployable, high-resolution, time-of-flight aerosol mass spectrometer, *Anal. Chem.*, *78*(24), 8281–8289.
DeCarlo, P. F., et al. (2010), Investigation of the sources and processing of organic aerosol over the Central Mexican Plateau from aircraft measurements during MILAGRO, *Atmos. Chem. Phys.*, *10*(12), 5257–5280.
Docherty, K. S., et al. (2011), The 2005 Study of Organic Aerosols at Riverside (SOAR-1): Instrumental intercomparisons and fine particle composition, *Atmos. Chem. Phys.*, *11*(23), 12,387–12,420.
Doshi, V., H. B. Vuthaluru, R. Korbee, and J. H. A. Kiel (2009), Development of a modeling approach to predict ash formation during co-firing of coal and biomass, *Fuel Process. Technol.*, *90*(9), 1148–1156.
Duan, F. K., X. D. Liu, T. Yu, and H. Cachier (2004), Identification and estimate of biomass burning contribution to the urban aerosol organic carbon concentrations in Beijing, *Atmos. Environ.*, *38*(9), 1275–1282.
Duan, F. K., K. B. He, Y. L. Ma, Y. T. Jia, F. M. Yang, Y. Lei, S. Tanaka, and T. Okuta (2005), Characteristics of carbonaceous aerosols in Beijing, China, *Chemosphere*, *60*(3), 355–364.
Dzepina, K., J. L. Jimenez, C. D. Cappa, R. M. Volkamer, S. Madronich, P. F. DeCarlo, and R. A. Zaveri (2011), Modeling the multiday evolution and aging of secondary organic aerosol during MILAGRO 2006, *Environ. Sci. Technol.*, *45*(8), 3496–3503.
Ge, X., A. Setyan, Y. Sun, and Q. Zhang (2012a), Primary and secondary organic aerosols in Fresno, California during wintertime: Results from high resolution aerosol mass spectrometry, *J. Geophys. Res.*, *117*, D19301, doi:10.1029/2012JD018026.
Ge, X., Q. Zhang, Y. Sun, C. R. Ruehl, and A. Setyan (2012b), Effect of aqueous-phase processing on aerosol chemistry and size distributions in Fresno, California, during wintertime, *Environ. Chem.*, *9*(3), 221–235.
Guo, S., et al. (2014), Elucidating severe urban haze formation in China, *Proc. Natl. Acad. Sci. U.S.A.*, *111*(49), 17,373–17,378.
Guo, Y., S. Li, Z. Tian, X. Pan, J. Zhang, and G. Williams (2013), The burden of air pollution on years of life lost in Beijing, China, 2004–08: Retrospective regression analysis of daily deaths.
Hayes, P. L., et al. (2013), Organic aerosol composition and sources in Pasadena, California, during the 2010 CalNex campaign, *J. Geophys. Res. Atmos.*, *118*, 9233–9257, doi:10.1002/jgrd.50530.
He, K., F. Yang, Y. Ma, Q. Zhang, X. Yao, C. K. Chan, S. Cadle, T. Chan, and P. Mulawa (2001), The characteristics of PM2.5 in Beijing, China, *Atmos. Environ.*, *35*(29), 4959–4970.
He, L. Y., Y. Lin, X. F. Huang, S. Guo, L. Xue, Q. Su, M. Hu, S. J. Luan, and Y. H. Zhang (2010), Characterization of high-resolution aerosol mass spectra of primary organic aerosol emissions from Chinese cooking and biomass burning, *Atmos. Chem. Phys.*, *10*(23), 11,535–11,543.
He, L. Y., X. F. Huang, L. Xue, M. Hu, Y. Lin, J. Zheng, R. Y. Zhang, and Y. H. Zhang (2011), Submicron aerosol analysis and organic source apportionment in an urban atmosphere in Pearl River Delta of China using high-resolution aerosol mass spectrometry, *J. Geophys. Res.*, *116*, D12304, 10.1029/2010JD014566.
He, L.-Y., M. Hu, X.-F. Huang, B.-D. Yu, Y.-H. Zhang, and D.-Q. Liu (2004), Measurement of emissions of fine particulate organic matter from Chinese cooking, *Atmos. Environ.*, *38*(38), 6557–6564.
Heald, C. L., J. H. Kroll, J. L. Jimenez, K. S. Docherty, P. F. DeCarlo, A. C. Aiken, Q. Chen, S. T. Martin, D. K. Farmer, and P. Artaxo (2010), A simplified description of the evolution of organic aerosol composition in the atmosphere, *Geophys. Res. Lett.*, *37*, L08803, doi:10.1029/2010GL042737.
Herndon, S. C., et al. (2008), Correlation of secondary organic aerosol with odd oxygen in Mexico City, *Geophys. Res. Lett.*, *35*, L15804, doi:10.1029/2008GL034058.
Hings, S. S., S. Walter, J. Schneider, S. Borrmann, and F. Drewnick (2007), Comparison of a quadrupole and a time-of-flight aerosol mass spectrometer during the Feldberg aerosol characterization experiment 2004, *Aerosol Sci. Technol.*, *41*(7), 679–691.
Hodzic, A., and J. L. Jimenez (2011), Modeling anthropogenically controlled secondary organic aerosols in a megacity: A simplified framework for global and climate models, *Geosci. Model. Dev.*, *4*(4), 901–917.
Hu, W. W., M. Hu, Z. Q. Deng, R. Xiao, Y. Kondo, N. Takegawa, Y. J. Zhao, S. Guo, and Y. H. Zhang (2012), The characteristics and origins of carbonaceous aerosol at a rural site of PRD in summer of 2006, *Atmos. Chem. Phys.*, *12*(4), 1811–1822.
Hu, W. W., et al. (2013), Insights on organic aerosol aging and the influence of coal combustion at a regional receptor site of central eastern China, *Atmos. Chem. Phys.*, *13*(19), 10,095–10,112.
Huang, R.-J., et al. (2014), High secondary aerosol contribution to particulate pollution during haze events in China, *Nature*, *514*(7521), 218–222.
Huang, X. F., L. Y. He, M. Hu, and Y. H. Zhang (2006), Annual variation of particulate organic compounds in PM2.5 in the urban atmosphere of Beijing, *Atmos. Environ.*, *40*(14), 2449–2458.
Huang, X. F., et al. (2010), Highly time-resolved chemical characterization of atmospheric submicron particles during 2008 Beijing Olympic Games using an aerodyne high-resolution aerosol mass spectrometer, *Atmos. Chem. Phys.*, *10*(18), 8933–8945.
Huang, X. F., L. Y. He, L. Xue, T. L. Sun, L. W. Zeng, Z. H. Gong, M. Hu, and T. Zhu (2012), Highly time-resolved chemical characterization of atmospheric fine particles during 2010 Shanghai World Expo, *Atmos. Chem. Phys.*, *12*(11), 4897–4907.
Jacob, D. J., B. D. Field, E. M. Jin, I. Bey, Q. Li, J. A. Logan, R. M. Yantosca, and H. B. Singh (2002), Atmospheric budget of acetone, *J. Geophys. Res.*, *107*(D10), 4100, doi:10.1029/2001JD000694.
Jimenez, J. L., et al. (2009), Evolution of Organic Aerosols in the Atmosphere, *Science*, *326*(5959), 1525–1529.
Kleinerman, R. A., Z. Wang, L. Wang, C. Metayer, S. Zhang, A. V. Brenner, S. Zhang, Y. Xia, B. Shang, and J. H. Lubin (2002), Lung cancer and indoor exposure to coal and biomass in rural China, *J. Occup. Environ. Med.*, *44*(4), 338–344.
Lanz, V. A., et al. (2008), Source attribution of submicron organic aerosols during wintertime inversions by advanced factor analysis of aerosol mass spectra, *Environ. Sci. Technol.*, *42*(1), 214–220.

Lee, A. K. Y., K. L. Hayden, P. Herckes, W. R. Leaitch, J. Liggio, A. M. Macdonald, and J. P. D. Abbatt (2012), Characterization of aerosol and cloud water at a mountain site during WACS 2010: Secondary organic aerosol formation through oxidative cloud processing, *Atmos. Chem. Phys.*, *12*(15), 7103–7116.

Lee, T., et al. (2010), Chemical smoke marker emissions during flaming and smoldering phases of laboratory open burning of wildland fuels, *Aerosol Sci. Technol.*, *44*(9).

Levin, E. J. T., et al. (2010), Biomass burning smoke aerosol properties measured during Fire Laboratory at Missoula Experiments (FLAME), *J. Geophys. Res.*, *115*, D18210, doi:10.1029/2009JD013601.

Lewis, K. A., et al. (2009), Reduction in biomass burning aerosol light absorption upon humidification: Roles of inorganically-induced hygroscopicity, particle collapse, and photoacoustic heat and mass transfer, *Atmos. Chem. Phys.*, *9*(22), 8949–8966.

Li, G., W. Lei, N. Bei, and L. T. Molina (2012), Contribution of garbage burning to chloride and PM2.5 in Mexico City, *Atmos. Chem. Phys.*, *12*(18), 8751–8761.

Li, J., M. Pósfai, P. V. Hobbs, and P. R. Buseck (2003), Individual aerosol particles from biomass burning in southern Africa: 2, Compositions and aging of inorganic particles, *J. Geophys. Res.*, *108*(D13), 8484, doi:10.1029/2002JD002310.

Li, Y. J., B. P. Lee, L. Su, J. C. H. Fung, and C. K. Chan (2015), Seasonal characteristics of fine particulate matter (PM) based on high-resolution time-of-flight aerosol mass spectrometric (HR-ToF-AMS) measurements at the HKUST Supersite in Hong Kong, *Atmos. Chem. Phys.*, *15*(1), 37–53.

Liang, L., G. Engling, F. Duan, Y. Cheng, and K. He (2012), Characteristics of 2-methyltetrols in ambient aerosol in Beijing, China, *Atmos. Environ.*, *59*, 376–381.

Lin, P., M. Hu, Z. Deng, J. Slanina, S. Han, Y. Kondo, N. Takegawa, Y. Miyazaki, Y. Zhao, and N. Sugimoto (2009), Seasonal and diurnal variations of organic carbon in PM2.5 in Beijing and the estimation of secondary organic carbon, *J. Geophys. Res.*, *114*, D00G11, doi:10.1029/2008JD010902.

Lovett, R. A. (2013), China's coal burning cutting lives short by years, *Nature news*.

Lundstedt, S., P. A. White, C. L. Lemieux, K. D. Lynes, I. B. Lambert, L. Öberg, P. Haglund, and M. Tysklind (2007), Sources, fate, and toxic hazards of oxygenated polycyclic aromatic hydrocarbons (PAHs) at PAH-contaminated sites, *Ambio*, *36*(6), 475–485.

McNeill, V. F., J. L. Woo, D. D. Kim, A. N. Schwier, N. J. Wannell, A. J. Sumner, and J. M. Barakat (2012), Aqueous-phase secondary organic aerosol and organosulfate formation in atmospheric aerosols: A modeling study, *Environ. Sci. Technol.*, *46*(15), 8075–8081.

Middlebrook, A. M., R. Bahreini, J. L. Jimenez, and M. R. Canagaratna (2012), Evaluation of composition-dependent collection efficiencies for the aerodyne aerosol mass spectrometer using field data, *Aerosol Sci. Technol.*, *46*(3), 258–271.

Millet, D. B., et al. (2010), Global atmospheric budget of acetaldehyde: 3-D model analysis and constraints from in-situ and satellite observations, *Atmos. Chem. Phys.*, *10*(7), 3405–3425.

Mohr, C., J. A. Huffman, M. J. Cubison, A. C. Aiken, K. S. Docherty, J. R. Kimmel, I. M. Ulbricht, M. Hannigan, and J. L. Jimenez (2009), Characterization of primary organic aerosol emissions from meat cooking, trash burning, and motor vehicles with high-resolution aerosol mass spectrometry and comparison with ambient and chamber observations, *Environ. Sci. Technol.*, *43*(7), 2443–2449.

Mohr, C., et al. (2012), Identification and quantification of organic aerosol from cooking and other sources in Barcelona using aerosol mass spectrometer data, *Atmos. Chem. Phys.*, *12*(4), 1649–1665.

Morgan, W. T., J. D. Allan, K. N. Bower, E. J. Highwood, D. Liu, G. R. McMeeking, M. J. Northway, P. I. Williams, R. Krejci, and H. Coe (2010), Airborne measurements of the spatial distribution of aerosol chemical composition across Europe and evolution of the organic fraction, *Atmos. Chem. Phys.*, *10*(8), 4065–4083.

Morino, Y., K. Tanabe, K. Sato, and T. Ohara (2014), Secondary organic aerosol model intercomparison based on secondary organic aerosol to odd oxygen ratio in Tokyo, *J. Geophys. Res. Atmos.*, *119*, 13,489–13,505, doi:10.1002/2014JD021937.

News, X. H. (2011), Beijing's population nears 20 million. [Available at http://www.chinadaily.com.cn/china/2011-05/05/content_12451856.htm.]

Ng, N. L., M. R. Canagaratna, J. L. Jimenez, P. S. Chhabra, J. H. Seinfeld, and D. R. Worsnop (2011a), Changes in organic aerosol composition with aging inferred from aerosol mass spectra, *Atmos. Chem. Phys.*, *11*(13), 6465–6474.

Ng, N. L., M. R. Canagaratna, J. L. Jimenez, Q. Zhang, I. M. Ulbrich, and D. R. Worsnop (2011b), Real-time methods for estimating organic component mass concentrations from aerosol mass spectrometer data, *Environ. Sci. Technol.*, *45*(3), 910–916.

Nuaaman, I., S. M. Li, K. L. Hayden, T. B. Onasch, P. Massoli, D. Sueper, D. R. Worsnop, T. S. Bates, P. K. Quinn, and R. McLaren (2015), Separating refractory and non-refractory particulate chloride and estimating chloride depletion by aerosol mass spectrometry in a marine environment, *Atmos. Chem. Phys. Discuss.*, *15*(2), 2085–2118.

Ortega, A. M., D. A. Day, M. J. Cubison, W. H. Brune, D. Bon, J. A. de Gouw, and J. L. Jimenez (2013), Secondary organic aerosol formation and primary organic aerosol oxidation from biomass-burning smoke in a flow reactor during FLAME-3, *Atmos. Chem. Phys.*, *13*(22), 11,551–11,571.

Paatero, P., P. K. Hopke, X. H. Song, and Z. Ramadan (2002), Understanding and controlling rotations in factor analytic models, *Chemom. Intell. Lab. Syst.*, *60*(1–2), 253–264.

Presto, A. A., M. A. Miracolo, J. H. Kroll, D. R. Worsnop, A. L. Robinson, and N. M. Donahue (2009), Intermediate-volatility organic compounds: A potential source of ambient oxidized organic aerosol, *Environ. Sci. Technol.*, *43*(13), 4744–4749.

Salcedo, D., et al. (2006), Characterization of ambient aerosols in Mexico City during the MCMA-2003 campaign with aerosol mass spectrometry: Results from the CENICA Supersite, *Atmos. Chem. Phys.*, *6*, 925–946.

Sheehan, P., E. Cheng, A. English, and F. Sun (2014), China's response to the air pollution shock, *Nat. Clim. Change*, *4*(5), 306–309.

Slowik, J. G., et al. (2010), Characterization of a large biogenic secondary organic aerosol event from eastern Canadian forests, *Atmos. Chem. Phys.*, *10*(6), 2825–2845.

Song, Y., Y. H. Zhang, S. D. Xie, L. M. Zeng, M. Zheng, L. G. Salmon, M. Shao, and S. Slanina (2006), Source apportionment of PM2.5 in Beijing by positive matrix factorization, *Atmos. Environ.*, *40*(8), 1526–1537.

Spracklen, D. V., et al. (2011), Aerosol mass spectrometer constraint on the global secondary organic aerosol budget, *Atmos. Chem. Phys.*, *11*(23), 12,109–12,136.

Streets, D. G., et al. (2007), Air quality during the 2008 Beijing Olympic Games, *Atmos. Environ.*, *41*(3), 480–492.

Sun, J. Y., Q. Zhang, M. R. Canagaratna, Y. M. Zhang, N. L. Ng, Y. L. Sun, J. T. Jayne, X. C. Zhang, X. Y. Zhang, and D. R. Worsnop (2010), Highly time- and size-resolved characterization of submicron aerosol particles in Beijing using an aerodyne aerosol mass spectrometer, *Atmos. Environ.*, *44*(1), 131–140.

Sun, Y. L., et al. (2011), Characterization of the sources and processes of organic and inorganic aerosols in New York City with a high-resolution time-of-flight aerosol mass apectrometer, *Atmos. Chem. Phys.*, *11*(4), 1581–1602.

Sun, Y. L., Z. F. Wang, P. Q. Fu, T. Yang, Q. Jiang, H. B. Dong, J. Li, and J. J. Jia (2013), Aerosol composition, sources and processes during wintertime in Beijing, China, *Atmos. Chem. Phys.*, *13*(9), 4577–4592.

Sun, Y., G. Zhuang, Y. Wang, L. Han, J. Guo, M. Dan, W. Zhang, Z. Wang, and Z. Hao (2004), The air-borne particulate pollution in Beijing—Concentration, composition, distribution and sources, *Atmos. Environ.*, *38*(35), 5991–6004.

Sun, Y., Z. Wang, H. Dong, T. Yang, J. Li, X. Pan, P. Chen, and J. T. Jayne (2012), Characterization of summer organic and inorganic aerosols in Beijing, China with an aerosol chemical speciation monitor, *Atmos. Environ.*, *51*, 250–259.
Sun, Y., Q. Jiang, Z. Wang, P. Fu, J. Li, T. Yang, and Y. Yin (2014), Investigation of the sources and evolution processes of severe haze pollution in Beijing in January 2013, *J. Geophys. Res. Atmos.*, *119*, 4380–4398, doi:10.1002/2014JD021641.
Takami, A., T. Miyoshi, A. Shimono, N. Kaneyasu, S. Kato, Y. Kajii, and S. Hatakeyama (2007), Transport of anthropogenic aerosols from Asia and subsequent chemical transformation, *J. Geophys. Res.*, *112*, D22S31, doi:10.1029/2006JD008120.
Takegawa, N., T. Miyakawa, Y. Kondo, J. L. Jimenez, Q. Zhang, D. R. Worsnop, and M. Fukuda (2006), Seasonal and diurnal variations of submicron organic aerosol in Tokyo observed using the Aerodyne aerosol mass spectrometer, *J. Geophys. Res.*, *111*, D11206, doi:10.1029/2005JD006515.
Takegawa, N., et al. (2009), Variability of submicron aerosol observed at a rural site in Beijing in the summer of 2006, *J. Geophys. Res.*, *114*, D00G05, doi:10.1029/2008JD010857.
Turpin, B. J., and H. J. Lim (2001), Species contributions to PM2.5 mass concentrations: Revisiting common assumptions for estimating organic mass, *Aerosol Sci. Technol.*, *35*(1), 602–610.
Turpin, B. J., and J. J. Huntzicker (1995), Identification of secondary organic aerosol episodes and quantitation of primary and secondary organic aerosol concentrations during SCAQS, *Atmos. Environ.*, *29*(23), 3527–3544.
Ulbrich, I. M., M. R. Canagaratna, Q. Zhang, D. R. Worsnop, and J. L. Jimenez (2009), Interpretation of organic components from positive matrix factorization of aerosol mass spectrometric data, *Atmos. Chem. Phys.*, *9*(9), 2891–2918.
Wang, L., Z. Liu, Y. Sun, D. Ji, and Y. Wang (2015), Long-range transport and regional sources of PM2.5 in Beijing based on long-term observations from 2005 to 2010, *Atmos. Res.*, *157*, 37–48.
Wang, Q., M. Shao, Y. Zhang, Y. Wei, M. Hu, and S. Guo (2009), Source apportionment of fine organic aerosols in Beijing, *Atmos. Chem. Phys.*, *9*(21), 8573–8585.
Wang, Z. B., M. Hu, D. L. Yue, J. Zheng, R. Y. Zhang, A. Wiedensohler, Z. J. Wu, T. Nieminen, and M. Boy (2011), Evaluation on the role of sulfuric acid in the mechanisms of new particle formation for Beijing case, *Atmos. Chem. Phys.*, *11*(24), 12,663–12,671.
Watson, J. G., J. C. Chow, and J. E. Houck (2001), PM2.5 chemical source profiles for vehicle exhaust, vegetative burning, geological material, and coal burning in Northwestern Colorado during 1995, *Chemosphere*, *43*(8), 1141–1151.
Wexler, A. S., and J. H. Seinfeld (1990), The distribution of ammonium salts among a size and composition dispersed aerosol, *Atmos. Environ. Part A*, *24*(5), 1231–1246.
Wood, E. C., et al. (2010), Investigation of the correlation between odd oxygen and secondary organic aerosol in Mexico City and Houston, *Atmos. Chem. Phys.*, *10*(18), 8947–8968.
Wu, Z. J., M. Hu, S. Liu, B. Wehner, S. Bauer, A. M. Ssling, A. Wiedensohler, T. Petaja, M. Dal Maso, and M. Kulmala (2007), New particle formation in Beijing, China: Statistical analysis of a 1-year data set, *J. Geophys. Res.*, *112*, D09209, doi:10.1029/2006JD007406.
Xu, J., Q. Zhang, M. Chen, X. Ge, J. Ren, and D. Qin (2014), Chemical composition, sources, and processes of urban aerosols during summertime in northwest China: Insights from high-resolution aerosol mass spectrometry, *Atmos. Chem. Phys.*, *14*(23), 12,593–12,611.
Xu, S., W. Liu, and S. Tao (2006), Emission of polycyclic aromatic hydrocarbons in China, *Environ. Sci. Technol.*, *40*(3), 702–708.
Yatavelli, R. L. N., et al. (2015), Estimating the contribution of organic acids to northern hemispheric continental organic aerosol, *Geophys. Res. Lett.*, *42*, 6084–6090, doi:10.1002/2015GL064650.
Yokelson, R. J., et al. (2009), Emissions from biomass burning in the Yucatan, *Atmos. Chem. Phys.*, *9*(15), 5785–5812.
Yuan, B., Y. Liu, M. Shao, S. Lu, and D. G. Streets (2010), Biomass burning contributions to ambient VOCs species at a receptor site in the Pearl River Delta (PRD), China, *Environ. Sci. Technol.*, *44*(12), 4577–4582.
Yuan, B., et al. (2012), Volatile organic compounds (VOCs) in urban air: How chemistry affects the interpretation of positive matrix factorization (PMF) analysis, *J. Geophys. Res.*, *117*, D24302, doi:10.1029/2012JD018236.
Yuan, B., W. W. Hu, M. Shao, M. Wang, W. T. Chen, S. H. Lu, L. M. Zeng, and M. Hu (2013), VOC emissions, evolutions and contributions to SOA formation at a receptor site in eastern China, *Atmos. Chem. Phys.*, *13*(17), 8815–8832.
Yue, D. L., M. Hu, R. Y. Zhang, Z. B. Wang, J. Zheng, Z. J. Wu, A. Wiedensohler, L. Y. He, X. F. Huang, and T. Zhu (2010), The roles of sulfuric acid in new particle formation and growth in the mega-city of Beijing, *Atmos. Chem. Phys.*, *10*(10), 4953–4960.
Zhang, J. K., Y. Sun, Z. R. Liu, D. S. Ji, B. Hu, Q. Liu, and Y. S. Wang (2014), Characterization of submicron aerosols during a month of serious pollution in Beijing, 2013, *Atmos. Chem. Phys.*, *14*(6), 2887–2903.
Zhang, Q. J., M. Beekmann, E. Freney, K. Sellegri, J. M. Pichon, A. Schwarzenboeck, A. Colomb, T. Bourrianne, V. Michoud, and A. Borbon (2015a), Formation of secondary organic aerosol in the Paris pollution plume and its impact on surrounding regions, *Atmos. Chem. Phys. Discuss.*, *15*(6), 8073–8111.
Zhang, Q., M. R. Canagaratna, J. T. Jayne, D. R. Worsnop, and J. L. Jimenez (2005a), Time- and size-resolved chemical composition of submicron particles in Pittsburgh: Implications for aerosol sources and processes, *J. Geophys. Res.*, *110*, D07S09, doi:10.1029/2004JD004649.
Zhang, Q., M. R. Alfarra, D. R. Worsnop, J. D. Allan, H. Coe, M. R. Canagaratna, and J. L. Jimenez (2005b), Deconvolution and quantification of hydrocarbon-like and oxygenated organic aerosols based on aerosol mass spectrometry, *Environ. Sci. Technol.*, *39*(13), 4938–4952.
Zhang, Q., J. L. Jimenez, D. R. Worsnop, and M. Canagaratna (2007a), A case study of urban particle acidity and its influence on secondary organic aerosol, *Environ. Sci. Technol.*, *41*(9), 3213–3219.
Zhang, Q., et al. (2007b), Ubiquity and dominance of oxygenated species in organic aerosols in anthropogenically-influenced Northern Hemisphere midlatitudes, *Geophys. Res. Lett.*, *34*, L13801, doi:10.1029/2007GL029979.
Zhang, Q., K. He, and H. Huo (2012), Policy: Cleaning China's air, *Nature*, *484*(7393), 161–162.
Zhang, Y. L., et al. (2015b), Fossil vs. non-fossil sources of fine carbonaceous aerosols in four Chinese cities during the extreme winter haze episode of 2013, *Atmos. Chem. Phys.*, *15*(3), 1299–1312.
Zhang, Y. X., J. J. Schauer, Y. H. Zhang, L. M. Zeng, Y. J. Wei, Y. Liu, and M. Shao (2008), Characteristics of particulate carbon emissions from real-world Chinese coal combustion, *Environ. Sci. Technol.*, *42*(14), 5068–5073.
Zhao, Y. L., M. Hu, S. Slanina, and Y. H. Zhang (2007), Chemical compositions of fine particulate organic matter emitted from Chinese cooking, *Environ. Sci. Technol.*, *41*(1), 99–105.
Zheng, B., Q. Zhang, Y. Zhang, K. B. He, K. Wang, G. J. Zheng, F. K. Duan, Y. L. Ma, and T. Kimoto (2014), Heterogeneous chemistry: A mechanism missing in current models to explain secondary inorganic aerosol formation during the January 2013 haze episode in North China, *Atmos. Chem. Phys. Discuss.*, *14*(11), 16,731–16,776.
Zheng, G. J., et al. (2015), Exploring the severe winter haze in Beijing: The impact of synoptic weather, regional transport and heterogeneous reactions, *Atmos. Chem. Phys.*, *15*(6), 2969–2983.
Zheng, M., L. G. Salmon, J. J. Schauer, L. M. Zeng, C. S. Kiang, Y. H. Zhang, and G. R. Cass (2005), Seasonal trends in PM2.5 source contributions in Beijing, China, *Atmos. Environ.*, *39*(22), 3967–3976.